SURFACE-CHARGE-TUNED VANADIA NANOWIRE PHOTOLYTIC HYDROGEN GENERATORS

By

SUNITH VARGHESE

Bachelor of Technology in Mechanical Engineering

Jawaharlal Nehru Technological University

Hyderabad, Telangana, India

2013

Submitted to the Faculty of the
Graduate College of the
Oklahoma State University
in partial fulfillment of
the requirements for
the Degree of
MASTER OF SCIENCE
July, 2016

SURFACE-CHARGE-TUNED VANADIA NANOWIRE PHOTOLYTIC HYDROGEN GENERATORS

Thesis Approved:

Dr. A. Kaan Kalkan

Thesis Advisor

Dr. Xiaoliang Jin

Dr. Ziad El-Rassi

ACKNOWLEDGEMENTS

First and above all, I thank God Almighty for guiding me in completing my thesis work successfully. Next, I thank my dearest mother, Sheela Varghese, for her unconditional love and countless sacrifices for me. I am forever indebted to you, whatever I am and whatever I will be, I owe it to you.

I express my deepest gratitude to my academic advisor, Dr. A. Kaan Kalkan, for his invaluable support, counsel and thoughtful guidance throughout my research work. I also thank my thesis defense committee members, Dr. Xiaoliang Jin and Dr. Ziad El-Rassi, for their support and feedback. I express my sincere thanks to Dr. Sadagopan. Krishnan and Charuksha Walgama for their assistance with cyclic voltammetry measurements.

Thank you to Özge Topal and Dr. Josh Ramsey for helping me with electrophoresis measurements. Thanks to Özge for helping me with my initial lab training as well. I am also indebted to my research colleagues, Sriharsha Karumuri and Linqi Zhang, for their invaluable suggestions and support. Additionally, I express my appreciation to Dr. Jean-Francois Veyan from the University of Texas at Dallas, for his help with ultraviolet photoelectron spectroscopy. Finally, I thank my family and friends, especially my father, brother-in-law, sister, niece, aunt, grandmother and my cousin Roshna, for their loving support, patience and encouragement.

Name: SUNITH VARGHESE

Date of Degree: JULY, 2016

Title of Study: SURFACE-CHARGE-TUNED VANADIA NANOWIRE PHOTOLYTIC HYDROGEN GENERATORS

Major Field: MECHANICAL AND AEROSPACE ENGINEERING

Abstract: The potential of hydrogen (H_2) is greater than most other fuels in terms of energy density and clean emissions. H_2 possesses an energy content per unit weight of 120 MJ/kg, three times that of gasoline. H_2 generation by photocatalytic splitting of water is considered as the most efficient way of producing a fully renewable and sustainable fuel. However, development of an efficient photocatalyst generating H_2 is challenged by a number of factors, one of which is efficient channeling of photogenerated electrons and holes to redox reactions. The present work investigates sol-gel synthesized vanadium oxyhydrate ($V_3O_7{\cdot}H_2O$) nanowires decorated with Au nanoparticles. Upon conjugation of vanadia nanowires with Au nanoparticles, the vanadia oxidizes to $V_2O_5{\cdot}H_2O$ with optical band gap changing from 2.3 eV indirect to 2.7 eV direct. Previously in our lab, reproducible conversion and external quantum efficiencies of 5.3% and 11.3% were demonstrated, respectively, using $V_2O_5{\cdot}H_2O$/Au nanoconjugates, as measured by gas chromatography for the first hour of photolysis under 470 nm excitation (8 mW/cm^2). Interestingly, a discrepancy was observed as the conduction band edge of $V_2O_5{\cdot}H_2O$ is determined to be 0.6 eV below standard H^+ reduction potential when measured by ultraviolet photoelectron spectroscopy (UPS), indicating H_2 reduction cannot be possible under normal conditions. Therefore, to explain the observed hydrogen generation, a hypothesis that the vanadia electron energy levels are being raised by some negative surface charge is put forth. In order to validate this hypothesis, cyclic current-voltage measurements were performed on aqueous suspensions of $V_3O_7{\cdot}H_2O$ nanowires and $V_2O_5{\cdot}H_2O$/Au nanoconjugates. The derived conduction and valence band edge energies exhibit exceptional consistency with optical band gaps, and also validate the hypothesized energy shift of the valence band by 1.9 and 1.6 eV, respectively. The negative surface charge is also corroborated by measured zeta potentials, determined to be −57.57 and −57.90 mV, respectively. Based on measured pH values of 2.5 and 2.4, respectively, the negative surface charge is attributed to Lewis acid nature of the nanowires, establishing coordinative bonding with OH^- adsorbates. The present work establishes that surface charge can be instrumental and enabling in photolytic fuel production.

TABLE OF CONTENTS

Chapter Page

LIST OF TABLES

Table Page

LIST OF FIGURES

Figure Page

CHAPTER 1

INTRODUCTION

World energy demand is rapidly increasing due to thriving global human population, which is estimated to be a staggering 9.8 billion by 2050, along with developing economic and social conditions [1]. Currently, 80% of the worldwide energy use is based on fossil fuels. However, fossil fuel reserves are rapidly depleting. In addition, usage of fossil fuels involves harmful greenhouse gas emissions such as carbon dioxide, nitrogen oxides, and aerosols etc., which pollute the environment. Hence, developing a clean and renewable energy source that can replace fossil fuels and meet the world's energy requirements is a pressing need.

Research efforts into this area has been of growing interest in the scientific community since the beginning of 1970's. Throughout history, mankind has made efforts to reduce the carbon:hydrogen (C:H) ratio in fuels. The next step in this endeavor is moving to a full hydrogen economy. The potential of hydrogen (H_2) in terms of energy density and clean emissions is greater than most other fuels. It has the highest energy content per unit weight among all fuels, 120 MJ/kg, which is three times that of gasoline [2]. When it is burned with oxygen, H_2 simply produces energy and water. The most economical and clean way of producing hydrogen is by the splitting of water, since water is ubiquitous on the earth's surface. A water molecule splits into hydrogen and oxygen when it is supplied with 1.23 eV energy. This process can be represented in the form of a basic water cycle as in Figure 1.1.

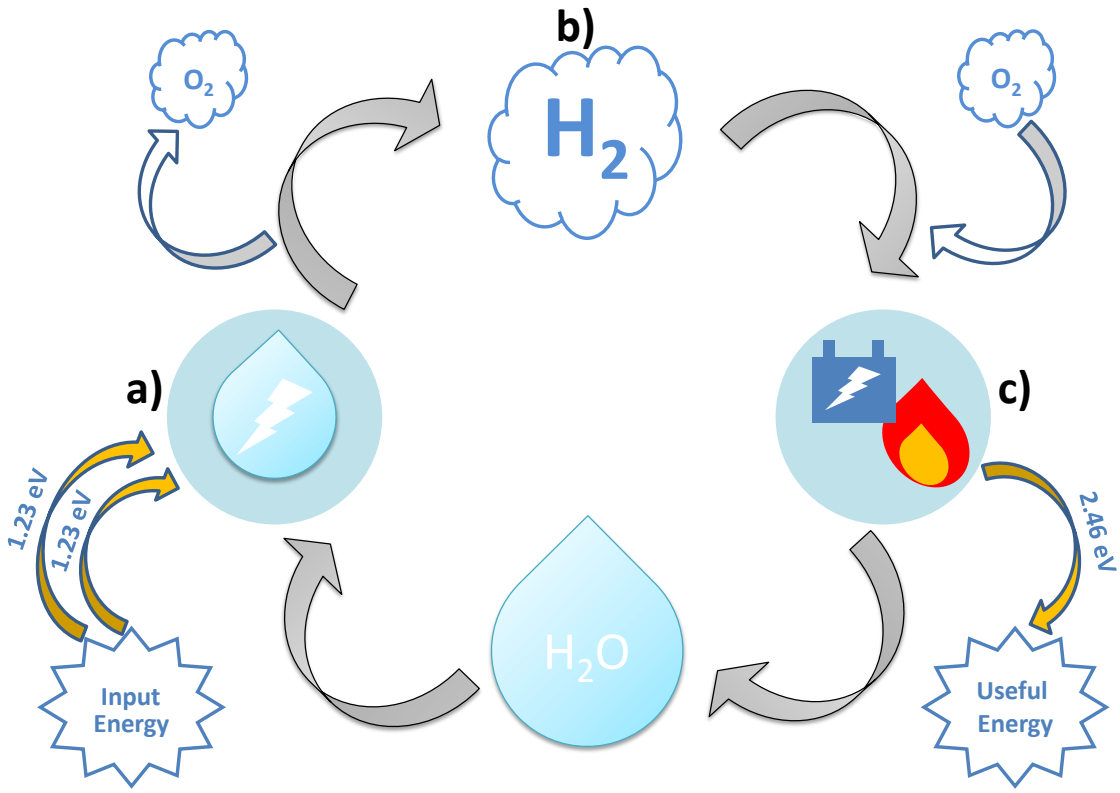

Figure 1.1: Illustration of water cycle showing energy of magnitude 1.23 eV supplied for the water splitting reaction into hydrogen and oxygen (a), production and storage of hydrogen (b), and hydrogen used in a fuel cell to convert it into useful energy (c) [Illustration adapted from http://www.en.rh2.org].

While there are other renewable energy resources which can supply the energy required for the splitting of water, solar energy is the most abundant energy resource on the earth. Of the sun's total radiation energy intercepted by the earth, about 60% reaches the earth's surface. Even if only 0.1% of this energy can be converted with an efficiency of 10% it would be four times the world's current energy generation of about 3,000 GW [3]. However, photolysis of water does not take place in nature when it is directly exposed to the radiation from the sun. Water does not absorb photon energies lower than 6.47 eV (>190nm). Of the sun's solar radiance spectrum, only

the ultraviolet region falls in this range of energy and it constitutes only about 5% of the sun's entire solar spectrum. To resolve this issue, a photocatalyst must be utilized, which can absorb photon energies in the visible light spectrum and channel a photogenerated electron-hole pair to the reduction and oxidation reactions to cleave a water molecule and form hydrogen and oxygen respectively. In this manner, photoelectrochemical (PEC) or photolytic cells function by employing a photocatalyst to absorb solar energy for the splitting of water and produce useful energy.

The oxidation half-cell reaction in this process is given by:

$$H_2O \rightarrow {}^{1}/_{2}\, O_2 + 2e^- + 2H^+$$

The reduction half-cell reaction of hydrogen is given by:

$$2e^- + 2H^+ \rightarrow H_2$$

The sum of these two reactions, namely the oxidation and reduction reactions gives the stoichiometric reaction for the splitting of water as described in the water cycle earlier:

$$H_2O \rightarrow H_2 + {}^{1}/_{2}\, O_2$$

The Gibbs energy change required to drive this water-splitting reaction is ΔG = 237.2 KJ/mol, which corresponds to ΔE = 1.23 V per electron-hole pair generated [4]. If this reaction is driven by light energy, the photocatalyst must absorb photon energies > 1.23eV and photogenerate two electron-hole pairs for every molecule of H_2. Hence, two photons of energy 1.23eV, which amounts to 2.46eV energy, are required for the photolytic splitting of water.

Photocatalytic splitting of water into hydrogen and oxygen was first demonstrated by Honda and Fujishima in 1972 using an n-type TiO_2 (rutile) photoanode and a platinum cathode

[5]. Several photocatalytic systems have been demonstrated since then, which produced H_2 by the splitting of water with varying quantum efficiencies (QEs). The highest QE of 56% has been reported for NiO-modified La/$KTaO_3$ using water under UV radiation [6]. Until recently, it was perceived that there was no material capable of the catalytic water splitting reaction under visible light with a QE greater than 10% [7]. This can be attributed to the challenge in finding a photocatalyst that fulfills all these four requirements: an efficient photocatalyst (a) should possess an optical band gap sufficient ($1.23 < E_g < 3.0$ eV) to effect the redox half-cell reactions and absorb visible light energies efficiently (b) should have efficient charge separation to avoid electron/hole recombination in its entire composition and effectively channel the electron/hole pair to the redox reaction active sites (c) should not be susceptible to photo-oxidation under light exposure (d) and should function under high overpotentials. A promising approach to enhance these photo-electric properties of photocatalysts is by the use of materials at the nanoscale.

In a previous attempt, a novel concept of a nanowire-nanoparticle (NW-NP) conjugate photolytic device was demonstrated by the Kalkan Lab, which exhibited reproducible conversion and external quantum efficiencies of 5.3% and 11.3% (measured by gas chromatography), respectively, for the first hour of photolysis under 470 nm (8 mW/cm^2) visible radiation [8]. The materials used for the synthesis of the photolytic nanodevice were vanadium oxyhydrate ($V_3O_7 \cdot H_2O$) with Au NPs decorating its surface. This effort produced H_2 with a significant QE under visible radiation using simple solution chemistry techniques for the material synthesis. However, further investigation is required. First, there was a lack of stability in the photolytic devices, which was seen by the degradation of photolysis after two hours of operation. Moreover, the reduction reaction cannot be explained by the energy band structure of vanadia in vacuum.

In this thesis work, the aforementioned NW-NP conjugate photolytic device is reconstructed and the mechanism of photolysis is studied further. Photocatalytic production of molecular hydrogen and oxygen using only water and visible light radiation of 470 nm (blue

light) wavelength is investigated. Interestingly, under normal conditions our nanoconjugates are not expected to reduce hydrogen, as the conduction band edge of vanadium oxyhydrate is too deep, that is, 5.1 eV below vacuum level when measured by ultraviolet photoelectron spectroscopy (UPS). To resolve this discrepancy and explain the observed hydrogen generation, further investigations were performed.

The main objective of the present thesis is to understand the mechanism of photolysis in this NW-NP conjugate photolytic device. To this end, the specific band structure of the photocatalyst employed, $V_3O_7 \cdot H_2O$ is investigated by means of UPS, optical absorption and cyclic voltammetry (CV) techniques. A proof of concept for the oxidation of the semiconductor precursor, $V_3O_7.H_2O$ to $V_2O_5.H_2O$ with optical band gap changing from 2.3 eV (indirect) to 2.7 eV (direct) is demonstrated. UPS was utilized to predict the positions of conduction and valence band edge energy levels of $V_3O_7.H_2O$ and $V_2O_5.H_2O$. We have hypothesized the lifting of vanadia energy levels by some negative surface charge to facilitate the hydrogen reduction reaction. To validate this hypothesis, cyclic current-voltage and electrophoresis measurements were performed on aqueous suspensions of $V_3O_7 \cdot H_2O$ nanowires and $V_2O_5 \cdot H_2O$ nanowires conjugated with Au nanoparticles. This gained understanding of the photolysis mechanism in the present semiconductor material establishes the importance of surface charge in enabling photolytic fuel production and may likely prove useful in the search for alternative photocatalyst materials as well.

The organization of the following chapters will be in this order. In Chapter 2, a brief summary of the background of photolysis will be presented. Additionally, past research efforts in the development of photolytic devices and main challenges in water photolysis are also examined. Furthermore, the materials used and experimental procedures utilized in the synthesis of the photolytic devices are outlined in Chapter 3. The results obtained during the course of this

investigation are presented and discussed in Chapter 4. Finally, the conclusions drawn from this present study will be detailed in Chapter 5.

CHAPTER 2

BACKGROUND

2.1 Photolysis of Water

Photolysis of water denotes hydrogen (H_2) production by cleaving a water molecule using photon energy. Hydrogen generation by photocatalytic water splitting can be considered as the best means of producing a fully renewable and sustainable fuel. As indicated in the preceding chapter, photolysis of water simply produces H_2 and O_2 and no harmful greenhouse gases are generated in the process. Moreover, solar insolation supplies the earth with a magnitude of power 10,000 times greater than the world's current power consumption [2]. A detailed review of the principles involved in the photocatalytic splitting of water is presented below.

2.1.1 Basic Principles of Heterogeneous Photocatalysis

Heterogeneous photocatalysis is the process in which the photocatalyst exists in a phase different from the reactants. Transition metal oxides and semiconductors are commonly employed in heterogeneous photocatalysis. A semiconductor possesses a band gap, preventing photogenerated electron/hole (e^-/h^+) pair recombination to occur too rapidly and allowing excited state lifetimes on the order of nanoseconds, unlike metals comprising a continuum of energy levels in which e^-/h^+ pair recombination can occur in the order of femtoseconds. This unique attribute in semiconductors leads to efficient photolysis, making them ideal for photocatalytic

applications. There are four basic steps involved in semiconductor photocatalysis. First, photons (e.g., solar irradiation) must be absorbed efficiently in the photocatalyst employed and generate an e^-/h^+ pair. Second, the photogenerated e^-/h^+ pair must be dissociated into constituent electrons (e^-) and holes (h^+). In the next step, the separated electrons and holes must be transported to the interfaces between water and the photocatalyst. The second and third steps are critical for efficient photolysis and must occur faster than other competing mechanisms like e^-/h^+ pair recombination. Fine particle size and high crystallinity promote efficient transport of charge carriers to the interfaces on account of shortened transport distances. In the final step, electrons and holes must be channeled to the redox reactions. Accordingly, the valence band edge of the photocatalyst (E_v) needs to be equal or deeper than −5.67 eV as measured from vacuum level, i.e. corresponding to a reduction potential of 1.23 eV or higher with respect to standard hydrogen electrode (SHE) potential in order to effect the oxidation reaction. Similarly, the conduction band edge (E_c) must be at an energy higher than −4.44 eV from vacuum level for the reduction reaction to occur at standard conditions. Based on these thermodynamic considerations, the band gap (E_g) of the employed semiconductor photocatalyst must be larger than 1.23 eV. However, when overpotentials are considered out of equilibrium, it is generally agreed that the bandgap should be larger than 1.5 eV.

2.1.2 Main Processes of Photocatalytic Water Splitting

Upon dissociation of the e^-/h^+ pair and transport to the redox reaction sites at the interfaces, they must participate in the reduction reaction of H^+ and oxidation of H_2O in order to photodissociate water molecules to produce H_2. The photogenerated h^+ created by photon energy ($h\upsilon$) absorption drives the oxidation of water at the photoanode as given by the equation:

$$2h^+ + H_2O \rightarrow {}^1/_2\, O_2 + 2H^+$$

Subsequently, the hydrogen reduction reaction takes place at the photocathode when the excited electrons (e^-) combine with H^+ ions (e.g., formed by the photodissociation of water), which is given by:

$$2e^- + 2H^+ \rightarrow H_2$$

The overall redox reaction is obtained by the summation of oxidation and reduction reactions stated above, which gives the stoichiometric equation for the splitting of water using a photocatalyst as:

$$2h\upsilon + H_2O \rightarrow H_2 + {}^1/_2\, O_2$$

For efficient water splitting under solar irradiation, a semiconductor photocatalyst which absorbs photons in the visible light spectrum (1.77 to 3.0 eV) must be utilized. Visible photon absorption by the photocatalyst is essential since almost half of the sun's solar radiance spectrum falls in the visible light range and barely 5% of the solar spectrum comprises UV light. Thus, combining this requirement with the one discussed in the previous section, the band gap (E_g) of the photocatalyst utilized should be between 1.5 eV and 3 eV ($1.5 < E_g < 3.0$ eV). The basic steps and main processes listed in this section should be faster than other competing mechanisms, such as photo-oxidation of the anode and e^-/h^+ pair recombination. Further, high overpotentials at the electrodes must be minimized. Additionally, photocatalyst stability in aqueous solutions is essential for a high photocatalytic output. An efficient visible-light-driven photocatalyst must possess all these requirements. Using photocatalysts at nanoscale dimensions eases migration of the photogenerated e^- and h^+ to the reduction and oxidation reaction sites due to shortened transport distances. Further, overpotentials are reduced as a result of high surface-to-volume ratio in conjunction with curvature-enhanced fields at the nanoscale [11].

2.2 Development of Photolytic Devices

Research interest in developing efficient photolytic devices was sparked by the discovery of the *Honda-Fujishima effect*, when the phenomenon of photocatalytic water splitting was first demonstrated by Honda and Fujishima using a TiO_2 (rutile) photoanode and a platinum (Pt) cathode under UV irradiation in 1972 [5]. Since then, fueled by an objective of finding a stable and efficient photocatalyst, more than 140 designs have been produced thus far [12]. However, most of these photocatalysts operate under UV light. Hitherto, discovering a photocatalyst operating in the visible light spectrum with a quantum efficiency (QE) greater than 10% has been very challenging [7]. Some of the important breakthroughs in the development of photolytic devices are outlined below.

2.2.1 TiO_2 Photocatalyst

TiO_2 is the most widely studied semiconductor photocatalyst since its discovery by Honda and Fujishima in 1972, due to its photo-chemical stability, relative abundance, non-toxicity and polymorphism. A schematic illustration of the PEC cell designed by Honda and Fujishima is presented in Figure 2.1. In this work, a semiconducting n-type, rutile (tetragonal crystal structure) TiO_2 photoanode in conjunction with a Pt cathode was used for photo-electrochemical water splitting under UV light exposure. A bias voltage was applied to support the reaction. The QE of the system was estimated to be 10%. Later, Park et al. reported that deposition of metals such as Au and Rh, and metal oxides such as Ni_2O_3 and CuO on TiO_2 enables visible light absorption in TiO_2 [13]. Additionally, composites of TiO_2 with an alternate catalyst enhanced the photocatalytic activity of TiO_2 by reducing the rate of e^-/h^+ pair recombination. This effect was reported by Georgieva et al., when they coupled WO_3 with TiO_2 to improve UV photocatalytic activity since the energy band diagram favored e^- transfer from the conduction band of TiO_2 to WO_3 for the H_2 reduction reaction [14].

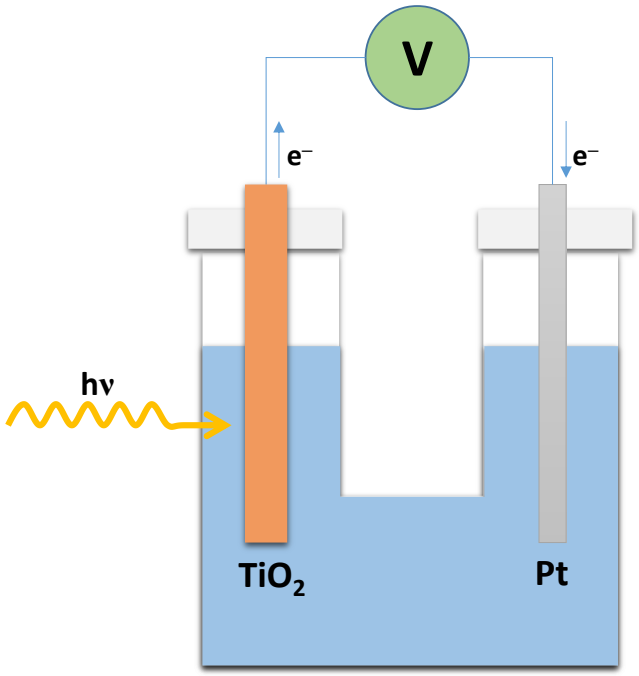

Figure 2.1: Photoelectrochemical cell designed by Honda and Fujishima in 1972 [Illustration adapted from reference 5].

In another effort, Zhang et al. reported that loading TiO_2 with CdS decreased recombination of e^-/h^+ pair effectively on account of its narrow band gap [15]. Kim et al. showed that NiO-modified TiO_2 catalyst enhanced H_2/O_2 evolution with a QE of 12% under UV irradiation. Further, doping TiO_2 with Ba and adding a sacrificial agent, NaOH to the suspension improved the QE significantly to about 35% [16]. Alternatively, Le et al. modified a composite, Co/TiO_2, surface using an inorganic dye, RhB dye, which produced a significant absorbance band in the range of 450-600 nm visible light and enhanced photocatalytic activity [17]. Structural modification of TiO_2, making use of improved properties at the nanoscale yielded higher H_2 photogeneration efficiency when compared to TiO_2 powder, as proved by Zhu and Zach [18] and Jitputti et al. [19]. Despite the progress made so far, the use of TiO_2 as a photocatalyst is limited by factors such as rapid e^-/h^+ pair recombination [20], large band gap of 3.2 eV restricting its use in the visible light region without the use of a co-catalyst and high overpotentials for H_2 photogeneration on TiO_2.

2.2.2 Metal Oxides

Several metal oxides have also been widely explored for photocatalytic applications based on their promising electronic properties. A study conducted by Kadowaki et al. produced hydrogen and oxygen evolution when RuO_2 was deposited onto $PbWO_4$ under UV irradiation [21]. Efficient photocatalytic splitting of water using a body centered-cubic (bcc) structure of VO_2 under UV light exposure was demonstrated by Wang et al. [22]. In another study, Zn-doped Ni/Ga_2O_3 proved to be an efficient photocatalyst under UV radiation, resulting in a quantum yield (QY) of 20% [23]. In an alternative study under visible light radiation, Maeda et al. observed that Rh-Cr mixed oxide coupled with GaN:ZnO allowed for photocatalytic water splitting with a 2.5% QE [24]. Zhu and Zach found that some of the commonly studied metal oxide photocatalysts have drawbacks such as ZnO, which easily undergoes photo-oxidation. While WO_3 is a stable photocatalyst under visible light irradiation with an optical band gap (E_g) of 2.7 eV, its conduction band edge energy level is lower than H_2 reduction potential. Hence, H_2 evolution cannot be made possible using WO_3 solely as a photocatalyst [18]. They also reported that using complex oxides, namely potassium hexaniobate ($NS\text{-}K_4Nb_6O_{17}$), perovskite ($ACa_2Nb_3O_{10}$, A=H or K) and $K_4Ce_2M_{10}O_{30}$ (M=Ta, Nb) as photocatalysts can enhance photocatalytic activity for water splitting.

2.2.3 Metal Sulfides

CdS is the most widely investigated metal sulfide due to its favorable band gap of 2.4 eV for visible light absorption below 510 nm wavelength and well-positioned valence and conduction band edges to effect the reduction and oxidation reactions for visible-light-driven splitting of water. Despite these advantages, CdS is easily photocorroded to Cd^{+2} and S (by the oxidation of S^{2-}) under prolonged light exposure. ZnS is another possible photocatalyst candidate but its band gap of 3.6 eV can absorb light only in the UV region. However, Cu-loaded ZnS

produced H_2 from aqueous Na_2SO_3 with a quantum yield of 3.7% under visible light illumination [25]. Additionally, Wu et al. outlined that alternate metal sulfide photocatalysts such as $CuInS_2$ and $AgInS_2$ can be used for H_2 and O_2 evolution under visible light irradiation by the use of sacrificial agents such as Na_2SO_3 and Na_2S [26]. Photocorrosion is the most widely encountered drawback in the use of metal sulfides as photocatalysts, along with band edge potentials not matching the requirements for water splitting.

2.2.4 Nanocomposites

Nanocomposite materials have exhibited significant improvements in photocatalytic efficiency for water splitting under visible light irradiation. In a study performed by Liu et al., TiO_2 intercalated with Au nanoparticles exhibited much higher H_2 generation under visible light exposure when compared with bare TiO_2 semiconductor [27]. In another attempt, CdS:ZnS/Au nanocomposite produced a significant improvement in photocatalytic activity when compared to photocatalysis without Au metal deposition [28]. Bao et al. reported a remarkable quantum yield of 60.34% for water photolysis using a Pt-loaded nanoporous CdS photocatalyst with sacrificial reagents, SO_3^{2-} and S^{2-} at 420 nm irradiation [29]. Other nanocomposites such as intercalated $Cd_{0.8}Zn_{0.2}S$ and Fe_2O_3 nanostructures have also been explored as possible photocatalyst materials [18]. A promising advantage of using nanocomposite photocatalysts is that photogenerated e^- can be transported to a co-catalyst with ease for the H_2 evolution reaction due to shorter transport distances, reducing the possibility of photogenerated e^-/h^+ pair recombination.

2.2.5 Z-scheme Photocatalysts

In a process inspired by natural photosynthesis in plants called Z-scheme photocatalysis, a two-step photocatalytic system is employed for water splitting in order to produce hydrogen. The first step in this process involves the O_2 evolution reaction and the next step is for H_2 evolution in the presence of a redox couple in solution. This technique reduces the energy

required for photocatalysis. Visible-light-driven photocatalysis was first demonstrated in 2005 using Z-scheme photocatalysis, in which TaON coupled with WO_3 enabled photocatalytic water splitting under visible light exposure with the help of a redox mediator, IO_3^-/I^- [30].

Some of the Z-scheme and nanocomposite (detailed in the previous section) photocatalysts can operate in the visible light region. However, most of them require the use of sacrificial reagents such as methanol or Na_2SO_3 for effecting the water splitting reaction, which are not eco-friendly and can prove to be a health hazard when used in large scale applications. In Table 2.1, some of the significant attempts in the development of photolytic water splitting devices are listed.

Table 2.1: Significant developments in the design of photolytic devices.

Photocatalyst	Designer	Year	QE/QY	Light Source
TiO_2, Pt	Honda/Fujishima [5]	1972	QE 10%	`UV
La/$NaTO_3$, NiO	Kato/Kudo [6]	2003	QY 56%	UV, 270 nm, 400 W
TiO_2, Ba	Kim/Lee [16]	2005	QE 35%	UV, 450 W
Ni/Zn-Ga_2O_3	Sakata/Matsuda [23]	2008	QE 20%	UV, 450 W
$(Ga_{1-x}Zn_x)(N_{1-x}O_x)$	Domen/Maeda [24]	2006	QE 2.5%	Visible, 420-440 nm
$Zn_{1-x}Cu_xS$	Kudo/Sekizawa [25]	1999	QY 3.7%	Visible, 420 nm, 300 W
CdS/Pt Nanocomposite	Bao/Shen [29]	2008	QY 60.34%	Visible, 420 nm, 300 W
TaON, WO_3 Z-scheme	Abe/Takata [30]	2005	QE 0.4%	Visible, 420 nm, 300 W

2.3 Main Challenges in Water Photolysis

Recent years have seen some notable progress in the development of photolytic devices. Nevertheless, finding a stable and efficient photocatalyst operating in the visible light regime is challenged by many factors. Some of the main challenges in water photolysis are enumerated below.

2.3.1 Photocatalyst Electrode Requirements

A functional photocatalyst electrode must fulfill four basic requirements: i) must have the appropriate energy band configuration, ii) must absorb photons efficiently, iii) must be resistant to photocorrosion, and iv) must have minimum overpotentials. These essential conditions for an effective photocatalyst electrode are detailed below.

1. For photo-electrochemical water splitting, energy band structure of the photocatalyst is of utmost importance. The conduction band edge must be higher than the H_2 reduction potential and the valence band edge must be lower than the H_2O oxidation reaction potential. In the case of an unsuitable energy band configuration, an external bias voltage will have to be applied to sustain the water splitting reaction.
2. The photoanode must absorb light in the visible spectrum efficiently. Direct and narrow band gap photoanodes enhance optical absorption of higher wavelength photons and generate more number of available e^-/h^+ pairs to accomplish the oxidation and reduction reactions for water splitting effectively.
3. Further, both cathode and anode must resist corrosion under continuous light exposure and in the presence of an electrolyte. The photoanode must be highly stable and enable oxidation of water without being oxidized itself. Most metal oxides satisfy this requirement but photoexcited e^-/h^+ pair recombination is high in some of these materials.

4. Finally, the semiconductor material should be able to operate under high overpotentials. The overpotentials of certain photocatalysts can be high for the H_2 evolution reaction, which reduces photocatalytic activity. The overpotential during electron transfer should be minimized to evade further photodegradation of the electrode.

2.3.2 Additional Factors Affecting Photolysis

In addition to the requirements that an efficient photocatalyst must satisfy, some other factors also affect photocatalytic efficiency. The morphology and crystallinity of the photocatalyst material can influence its properties. Crystallinity in a photocatalyst results in higher carrier mobilities, which ease the transport of photogenerated e^-/h^+ pair to the interfaces. Additionally, Meshram et al. claimed that planar CuO crystals absorbed light irradiation to a greater extent when compared with spherical CuO crystals, emphasizing the effect of morphology on light absorption [31]. Usage of sacrificial reagents that act as h^+ or e^- scavengers in redox reactions can improve photocatalytic activity. Methanol or ethanol are most commonly used sacrificial agents. Higher light intensity can increase photolytic efficiency by generating more number of e^-/h^+ pairs for consumption by redox reactions instead of recombining. Finally, the solution pH can affect photolysis of water. Jiang et al. [32] and Hoffmann et al. [33] showed that a change in the solution pH can alter band edge potentials in order to effect water splitting reactions. Further, Nada et al. demonstrated that H_2 evolution was greater in acidic medium than in basic medium using a TiO_2/RuO_2 photocatalyst in the presence of methanol reagent [34]. The reason for this improvement is that in an acidic medium, more number of H^+ ions are adsorbed on the electrode surface, which increases the probability of H_2 reduction on TiO_2 surface.

2.4 Photocatalyst Employed in the Present Work

The photocatalyst material used in the present work consists of conjugates of vanadium oxyhydrate ($V_3O_7 \cdot H_2O$) nanowires and Au nanoparticles. Vanadium oxyhydrate NWs are

synthesized using sol-gel technique and Au NPs are decorated on $V_3O_7{\cdot}H_2O$ NW surfaces by chemical reduction. Previously, these nanoconjugate devices were synthesized in the Kalkan Lab. Further, they measured reproducible light-to-hydrogen conversion and external quantum efficiencies of 5.3% and 11.3% using gas chromatography, respectively, for the first hour of photolysis under 470 nm (8 mW/cm^2) radiation [35].

$V_3O_7{\cdot}H_2O$ is a transition metal oxide hydrate, in which vanadium exists in its oxidation states of +4 and +5. $V_3O_7{\cdot}H_2O$ is a dark green semiconductor material with a band gap suitable for visible light absorption. In the aforementioned previous work, scanning electron microscopy (SEM) studies performed on vanadia nanowires revealed a dense collection of NWs, analogous to a "bird's nest" structure in the aerogel form. After dispersing in water, the average diameter of the nanowires was found to be 9±2 nm. Further, a transmission electron microscopy (TEM) study conducted subsequent to Au NP reduction revealed a low contact angle of Au NPs, demonstrating a strong adhesion of Au on vanadia NW surfaces. The majority of the Au NPs were found to be smaller than 5 nm in size. TEM images of the vanadia nanowires and nanoconjugates are shown in Figure 2.2 [35].

In another study of the Kalkan Lab, Topal et al. conducted X-ray diffraction (XRD) of the $V_3O_7{\cdot}H_2O$ nanowires, determining its structure to be orthorhombic crystalline structure. Additionally, a high resolution TEM image of a single nanowire showed that the nanowires exhibit high crystallinity [36]. On the other hand, as revealed in the present work and as will be elaborated in Chapter 4, the nanowires are found to transform to $V_2O_5{\cdot}H_2O$ upon Au reduction. Au particles provide efficient cathodic sites for the H_2 evolution reaction. The precise role of Au NPs in enhancing photocatalytic activity will be presented in Chapter 4. The present thesis further investigates the mechanisms of photolytic H_2 generation using $V_2O_5{\cdot}H_2O$/Au nanowire/nanoparticle conjugates. Moreover, the reduction reaction could not be explained earlier by the energy band structure of vanadia in vacuum. To this end, ultraviolet photoelectron

spectroscopy (UPS), optical absorption spectroscopy and cyclic voltammetry (CV) were performed to further explicate the electron energy band structure of the vanadia nanowires in vacuum as well as in aqueous solution.

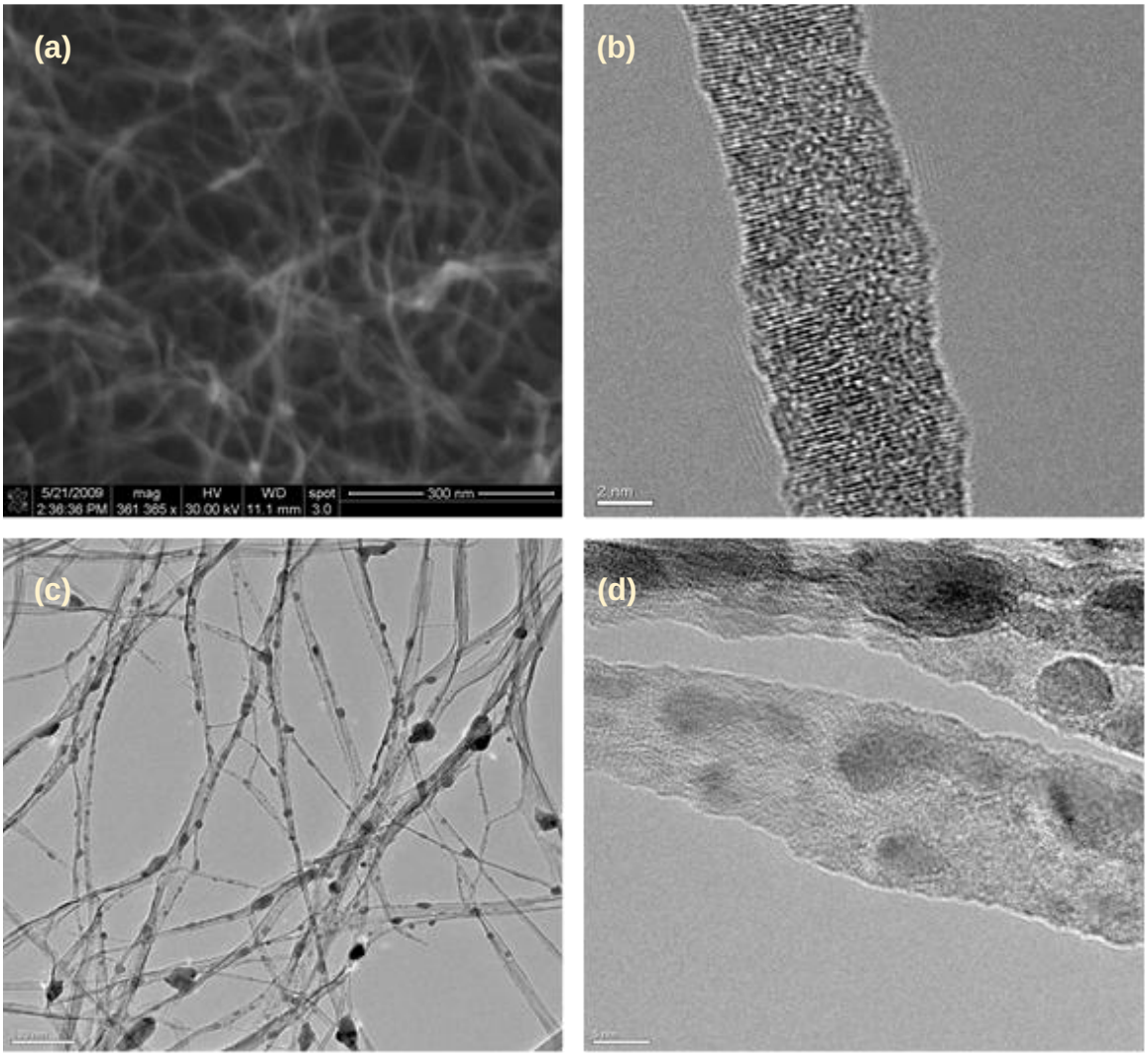

Figure 2.2: TEM image of sol-gel synthesized $V_3O_7{\cdot}H_2O$ nanowires (a). High resolution TEM image of a single $V_3O_7{\cdot}H_2O$ NW (b). TEM image of Au-decorated vanadia nanowires. The darker dots in the image represent the Au NPs (c). High resolution TEM image of vanadia/Au nanoconjugates (d) [35, reprinted with permission].

2.5 Important Definitions Pertaining to Photolytic Efficiencies

External Quantum Efficiency (EQE) is defined as the ratio of number of electron/hole pairs involved in photolysis redox reactions to the number of incident photons. For calculations of EQE in water photolysis, the number of instrumental electron/hole pairs are given by twice the number of moles of H_2 generated multiplied by the Avogadro constant.

$$EQE = \frac{\#\ of\ instrumental\ electron\ and\ hole\ pairs}{\#\ of\ incident\ photons}$$

$$EQE = \frac{2 \times n_{H_2} \times N_A}{\#\ of\ incident\ photons}$$

Internal Quantum Efficiency (IQE) is the ratio of number of electron/hole pairs involved in photolysis redox reactions to the number of absorbed photons (i.e., number of electron/hole pairs generated).

$$IQE = \frac{\#\ of\ instrumental\ electron\ and\ hole\ pairs}{\#\ of\ absorbed\ photons}$$

Finally, light-to-H_2 conversion efficiency (LTHE) or solar-to-H_2 conversion efficiency (STHE) is defined as the ratio of electromagnetic energy stored as chemical energy in H_2 during photolysis to incident electromagnetic energy over a certain time period.

$$LTHE = \frac{total\ chemical\ energy\ stored\ in\ H_2}{total\ incident\ electromagnetic\ energy}$$

CHAPTER 3

METHODOLOGY

3.1 Synthesis of Nanoconjugates

3.1.1 Sol-Gel Synthesis of $V_3O_7 \cdot H_2O$ Nanowires

Vanadium oxyhydrate ($V_3O_7 \cdot H_2O$) nanowires were synthesized by sol-gel technique. First, 9.5 mL of acetone are mixed with 4.7 mL of deionized (DI) water in a vial. Second, 2 mL of vanadium tripropoxide, $\{VO(OCH_2CH_2CH_3)_3\}$, are drawn into a second vial. The aforementioned volumes of chemicals were determined based on ease of fabrication since this technique is a time-sensitive process. Next, both vials were closed and cooled in a solid-CO_2/acetone bath (−78 ^oC) till ice chunks start forming in the water/acetone mixture and vanadium tripropoxide solution becoming highly viscous. This step is performed in order to slow down the gelation process. Prior to mixing of the precursors, the water/acetone solution is shaken vigorously by hand to minimize the ice chunks. Subsequently, the water/acetone solution was added to vanadium tripropoxide and immediately the mixture was shaken vigorously for 10-15 s. This step ensures that both solutions combine homogeneously upon mixture. Thereafter, the formed ‘sol’ was quickly transferred to vertically pre-positioned polyethylene syringes (Becton Dickinson & Co., Luer-LokTM Tip, 10mL). The syringes were then sealed at both ends using syringe plungers leaving 0.5 mL air head space above the wet gels. Next, the ‘sol’ was left for complete gelation for 5 days in the syringes.

The setup for drying wet gels in syringes with the two-plunger system can be seen in Figure 3.1.

Figure 3.1: Multiple wet 'sol' gels after mixture of vanadium tripropoxide and water/acetone solution; subsequently left for aging for 5 days.

Upon aging, the wet gels were transferred to bottles containing anhydrous acetone 8-10 times the gel volume. To wash off the excess precursors and byproducts, the acetone was

changed every 12 hours for 5 days. Finally, the gels were ambient dried at standard temperature and pressure (STP) conditions to evaporate the exchanged acetone (until shrinking to $1/10^{th}$ of their original size). The obtained aerogels are dull green and fragile in appearance. A flowchart enumerating the various steps involved in the sol-gel synthesis of $V_3O_7{\cdot}H_2O$ nanowires is presented in Figure 3.2.

3.1.2 Fabrication of $V_2O_5{\cdot}H_2O$/Au nanoconjugates

After ambient drying, the $V_3O_7{\cdot}H_2O$ aerogel was dispersed in DI water at a concentration of 3.4 g/L by vortex mixing for several minutes. The nanowire suspension was then stored in an amber bottle for at least a day before further processing. The fabrication of the photolytic nanodevice suspension involved reduction of Au nanoparticles (NPs) on the $V_3O_7{\cdot}H_2O$ nanowires. Accordingly, 0.2 mL of tetrachloroauric acid, $HAuCl_4$ (0.1 M) is diluted in 2 mL of DI water and added to 2 mL of $V_3O_7.H_2O$ (3.4 g/L) and the mixture was shaken vigorously. Afterwards, the mixture was left undisturbed for at least 16 h before photolysis or any materials characterization. The synthesized NW/NP conjugate photolytic device suspension consists of 5.0 mM $HAuCl_4$, and 1.7 g/L of $V_2O_5{\cdot}H_2O$ nanowires. A flowchart indicating the steps associated with the process for decoration of Au nanoparticles on $V_2O_5{\cdot}H_2O$ nanowires is shown in Figure 3.3. The nanostructure suspension before and after Au reduction can be seen in 20 mL glass vials in Figures 3.4a and 3.4b, respectively.

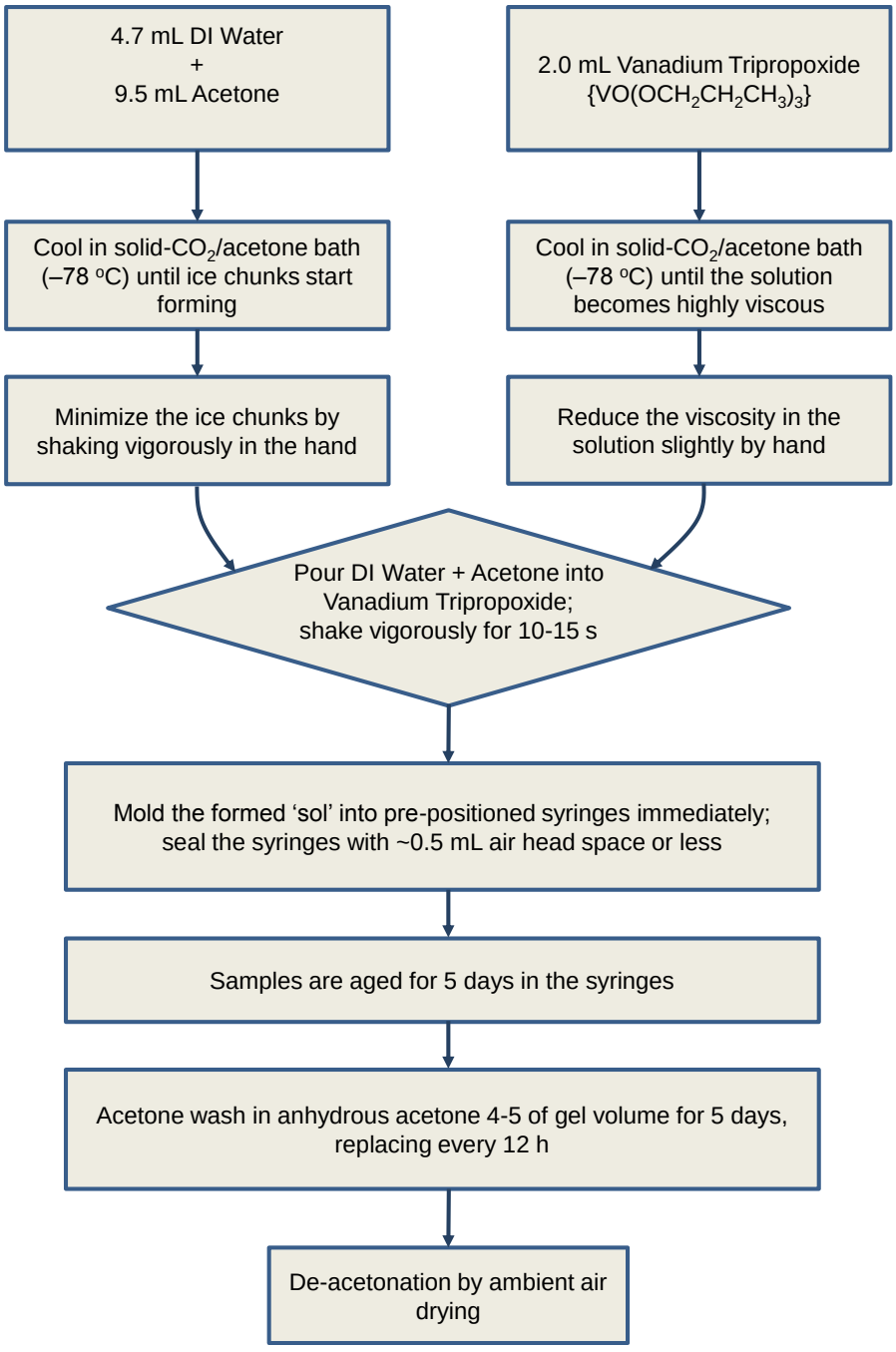

Figure 3.2: Flowchart listing the steps involved in the sol-gel synthesis of $V_3O_7 \cdot H_2O$ nanowires.

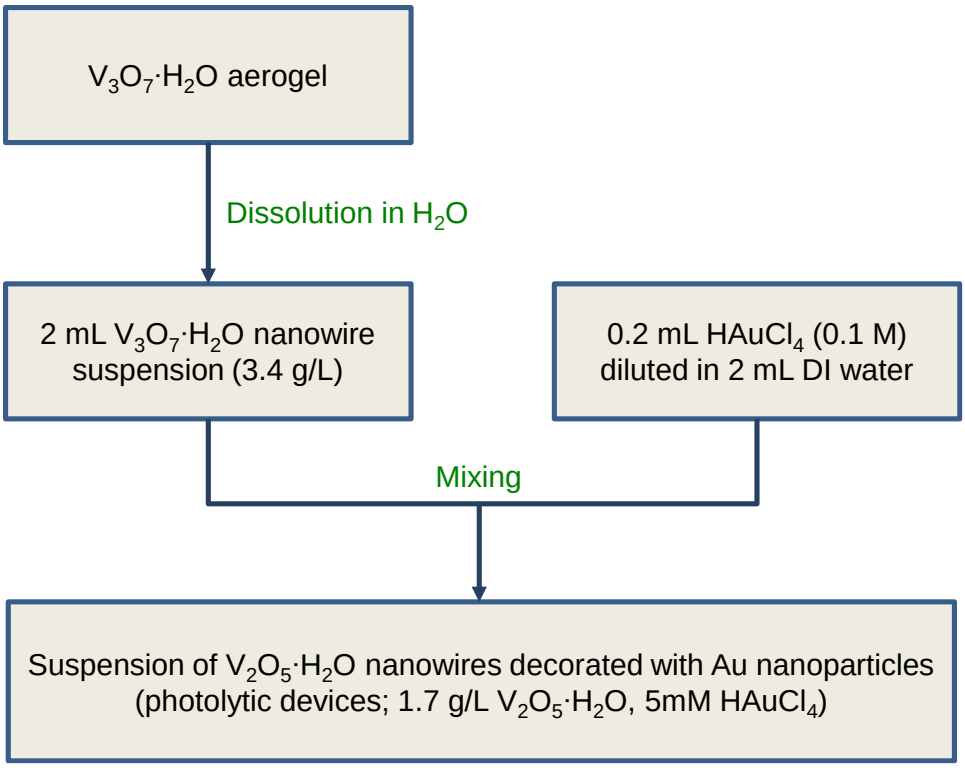

Figure 3.3: Flowchart listing the process steps for decoration of $V_2O_5{\cdot}H_2O$ nanowires with Au nanoparticles (fabrication of photolytic devices).

3.2 Materials Characterization

3.2.1 Ultraviolet-Visible Spectroscopy

In order to investigate the optical properties of $V_3O_7{\cdot}H_2O$ nanowires as well as $V_2O_5{\cdot}H_2O$/Au nanoconjugates, UV-visible spectroscopy was used. The optical absorption data were acquired by a double beam Varian Cary 300 Bio UV-visible spectrophotometer (Agilent Technologies, Wilmington, DE). The instrument measures the transmittance of a sample (T), which is the ratio between transmitted intensity of the incident light (I) and intensity of incident light before passing through the sample at a given wavelength (I_o).

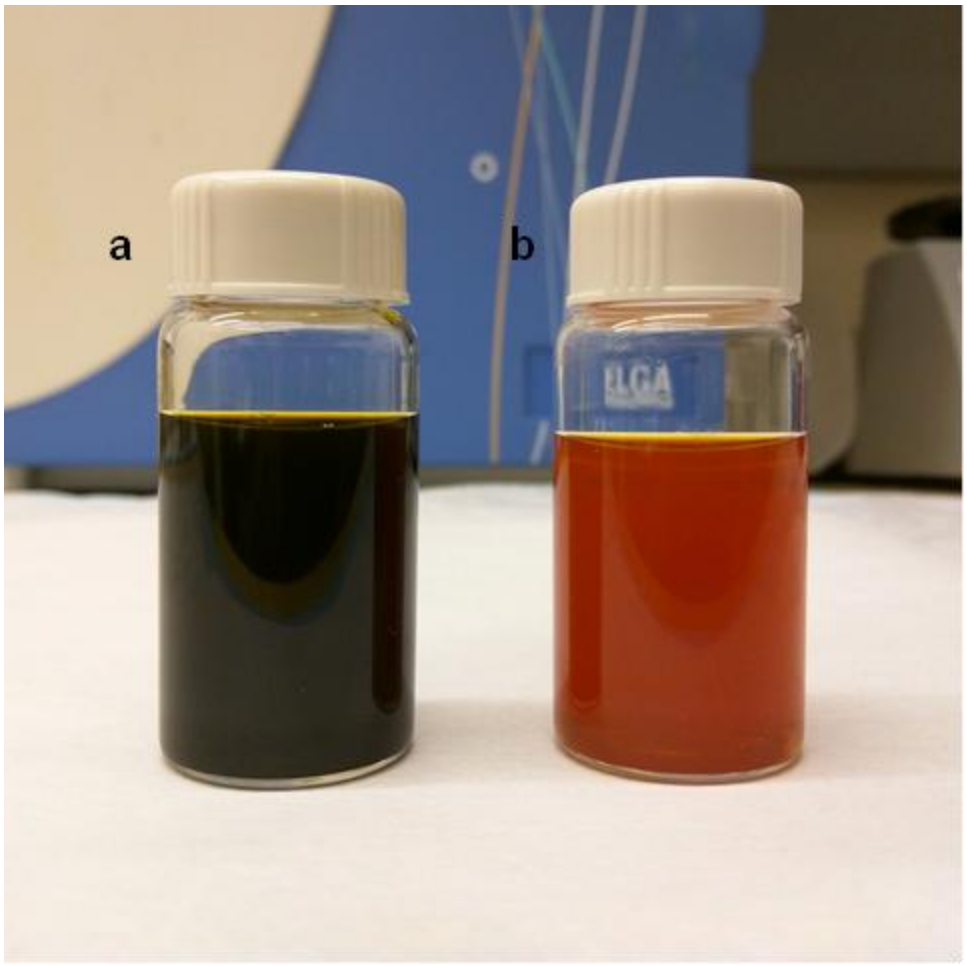

Figure 3.4: $V_3O_7.H_2O$ nanowire suspension at 3.4 g/L concentration (a); $V_2O_5{\cdot}H_2O$/Au nanoconjugate suspension synthesized with 5.0 mM $HAuCl_4$ and 1.7 g/L $V_2O_5{\cdot}H_2O$ concentrations (b).

The reference beam intensity is considered as 100% transmittance (or 0% absorption), and the quantity obtained is the ratio of the two beam intensities. The absorbance, A, is then determined by taking the negative logarithm of transmittance as:

$$A = -\log(T) = -\log\left(I/I_0\right)$$

For the acquisitions, the $V_3O_7{\cdot}H_2O$ stock suspension (3.4 g/L) was diluted 30 times and as-prepared conjugate suspensions were diluted by 15 times in order to enhance the signal-to-noise ratio. Absorbance measurements were performed with the samples enclosed in quartz glass

cuvettes (optical path length of 1 cm) and referenced to DI water. The wavelength range of the scans were from 200 to 800 nm. Acquisitions were performed with an integration time of 0.1 s at 1 nm intervals. To remove any background due to instrument and acquire reliable data, baseline correction was performed before each measurement.

3.2.2 Band Gap Determination using Tauc Plots

For the derivation of band gap energies (E_g) of $V_3O_7{\cdot}H_2O$ nanowires as well as Au-decorated $V_2O_5{\cdot}H_2O$ nanowires using Tauc plots, optical absorbance data obtained by UV-Vis spectroscopy as described in the previous section was used. For the calculations, the optical absorbance data were acquired at 30 times dilution of $V_3O_7{\cdot}H_2O$ nanowires suspension and 15 times dilution of as-prepared conjugate suspension. Next, in order to generate the Tauc plots, the wavelength (nm) on the abscissa axis was converted to photon energy (eV). Further, optical absorbance on the ordinate axis is converted to the quantity $(\alpha h\upsilon)^{1/2}$ in the case of $V_3O_7{\cdot}H_2O$ nanowires and $(\alpha h\upsilon)^2$ for $V_2O_5{\cdot}H_2O$/Au nanoconjugates, where 'α' represents the absorption coefficient (or absorbance) obtained from the UV-Vis spectroscopy data, 'h' is Planck's constant and 'υ' is the frequency of the incident light radiation. The quantity $(\alpha h\upsilon)^{1/2}$ is used to identify indirect allowed transitions and $(\alpha h\upsilon)^2$ is used to identify direct allowed transitions. Baseline correction was performed prior to Tauc plots. The obtained plot has a distinct linear regime, which determines the onset of absorption upon extrapolation to intercept the x-axis (photon energy). In other words, a straight line is fit to the linear regime and the point of intersection with the abscissa is adopted as the optical band gap.

3.2.3 Ultraviolet Photoelectron Spectroscopy

Ultraviolet photoelectron spectroscopy (UPS) measurements were performed in order to determine the ionization energies, namely valence band edge energies of $V_3O_7{\cdot}H_2O$ nanowires and $V_2O_5{\cdot}H_2O$/Au nanoconjugates. The UPS was performed using a Physical Electronics PHI

Versa Probe II system with He I excitation (21.2 eV) with a substrate bias of 6 V. The lower energy of photons from a UV light source (21.2 eV) when compared to higher energy X-rays used in X-ray photoelectron spectroscopy (200-2000 eV), ensures that only the electrons from the outermost energy levels, namely the valence band edge are ionized. An electron energy analyzer is used to measure the kinetic energy of the free electrons. Thereafter, the binding energy (BE) of the electrons is calculated as the difference between the UV photon energy (hυ) and kinetic energy of excited electrons (KE). This relation is given by:

$$BE = h\upsilon - KE$$

The samples for UPS measurements were prepared by immersion coating. Copper (Cu) substrates of an average size 12 × 12 mm^2 were polished using 0.3-µm Al_2O_3 slurry, followed by rinse with DI water and isopropyl alcohol. Next, the substrates were sonicated in DI water for 5 min. Subsequently, the Cu substrates were immersed in $V_3O_7{\cdot}H_2O$ (1.7 g/L) and $V_2O_5{\cdot}H_2O$/Au (2× diluted from as-synthesized) suspensions for 130 and 80 s, respectively, followed by ambient drying. Measurements were performed after 5 min of sputter clean as UPS is a surface sensitive technique. All measurements were acquired in an ultrahigh vacuum environment to avoid any attenuation in output signal due to interaction with ambient air.

3.2.4 Cyclic Voltammetry

To validate the hypothesis of lifting of vanadia electron energy levels, cyclic voltammetry (CV) measurements were performed on aqueous suspensions of $V_3O_7{\cdot}H_2O$ nanowires and $V_2O_5{\cdot}H_2O$ nanowires conjugated with Au nanoparticles. For data acquisition, a standard three-electrode electrochemical cell (CH instruments, Model CHI 6017, Austin, TX) consisting of a Ag/AgCl reference electrode (1 M KCl, CH Instruments), a Pt-wire counter electrode and a high-purity graphite (HPG) disk working electrode. Prior to a CV measurement, the HPG working electrode was polished by using a 0.3-µm Al_2O_3 slurry, followed by DI

water/ethanol rinse and sonication in DI water for 30s. The CV data were acquired for stock and as-synthesized concentrations of the $V_3O_7 \cdot H_2O$ nanowires and $V_2O_5 \cdot H_2O$/Au nanoconjugates, respectively, without dilution. No auxiliary electrolyte was employed due to high conductivity of the suspensions. The derived parameters from CV data were averaged for 5 measurements for both $V_3O_7 \cdot H_2O$ nanowires and $V_2O_5 \cdot H_2O$/Au nanoconjugates. Cyclic voltammograms were acquired at 25 °C and a scan rate of 0.1 V/s after Ar purging for 5 min to remove any dissolved oxygen. The measurement setup for cyclic voltammetry is shown in Figure 3.5.

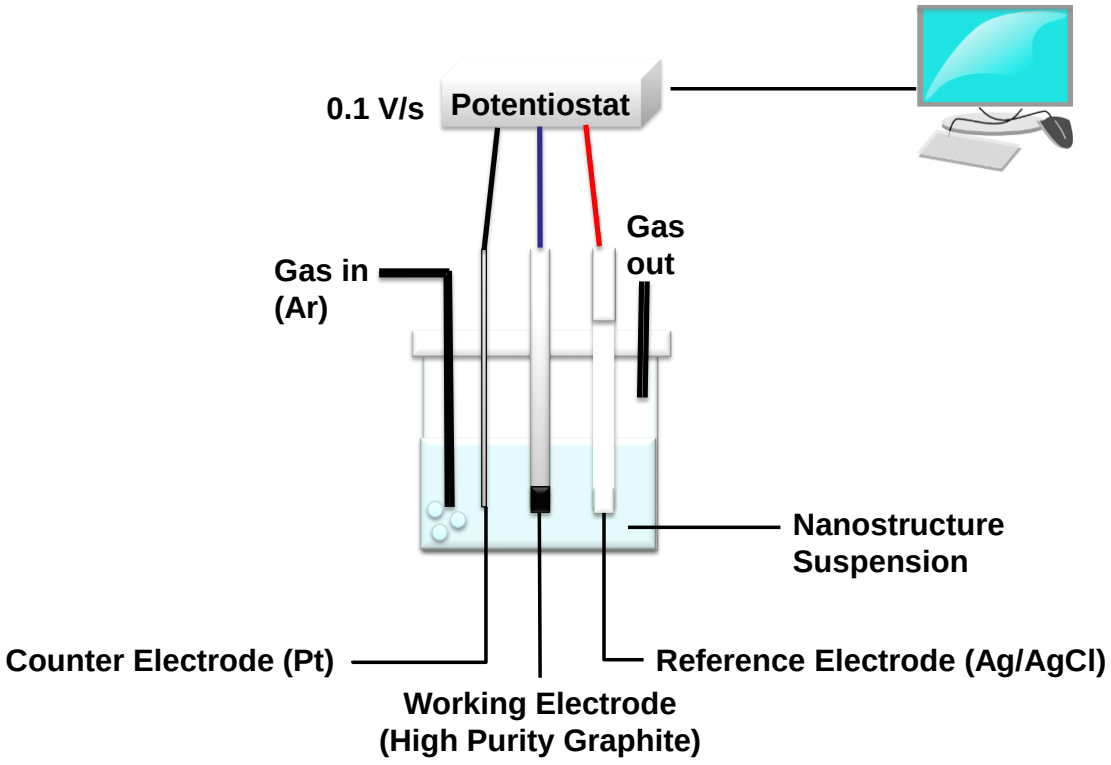

Figure 3.5: Standard three-electrode electrochemical cell setup for cyclic voltammetry measurements.

3.2.5 Electrophoresis

To support the hypothesis of lifting up of energy levels in $V_3O_7 \cdot H_2O$ and vanadia/Au nanostructures by a certain negative surface charge, ζ-potentials of the nanostructures were measured using electrophoresis. Measurements were acquired using a ZetaPALS Brookhaven Instruments Corporation ζ-potential analyzer. ζ-potentials quantify the electrokinetic potential difference between the surface of the nanostructures and the dispersion medium. According to the double layer model, ζ-potentials are measured as the electric potential difference at the location of the slip plane relative to a point in the dispersion medium. Though ζ-potential values are not equal to the electric surface potentials, ζ-potentials are a fair approximation to characterize the magnitude of the surface charge. ζ-potential values were averaged and presented after 10 measurements.

CHAPTER 4

RESULTS AND DISCUSSION

4.1 Band Gap of Vanadia Nanowires before and after Au Nanoparticle Conjugation

The band gap energies (E_g) of $V_3O_7 \cdot H_2O$ NWs and vanadia NWs conjugated with Au NPs after reduction were determined using Tauc plots. The band gap energies are derived from optical absorbance data obtained by UV-visible spectroscopy. The optical absorbance data acquired for $V_3O_7 \cdot H_2O$ NWs and vanadia/Au nanoconjugates are shown in Figures 4.1a and 4.1b, respectively. Next, Tauc plots were generated from the obtained optical absorbance spectra using the method described in section 3.2.2. From the Tauc plots, the point of intersection of a straight line fit to the distinct linear regime and the photon energy on abscissa axis is adopted as the optical band gap. This extrapolated point on the graph at which the optical absorbance tends to 0 can be anticipated as the band gap. Figures 4.2a and 4.2b depict Tauc plots of vanadia NWs before and after conjugation with Au NPs, respectively. In the figures, the band gap energy is indicated by a dotted line.

As seen from Fig. 4.2, the band gap of $V_3O_7 \cdot H_2O$ NWs (before reduction) is found to be 2.28 eV indirect. On the other hand, the band gap increases to 2.69 eV and changes to direct after Au reduction on the nanowires. This change in E_g of the nanowires after Au NP reduction is indicative of a change in the crystal and/or chemical structure. Upon comparison with the optical absorption data obtained by Escobar *et al.* [37], an inference can be drawn that $V_3O_7 \cdot H_2O$ oxidizes to $V_2O_5 \cdot H_2O$ upon Au reduction.

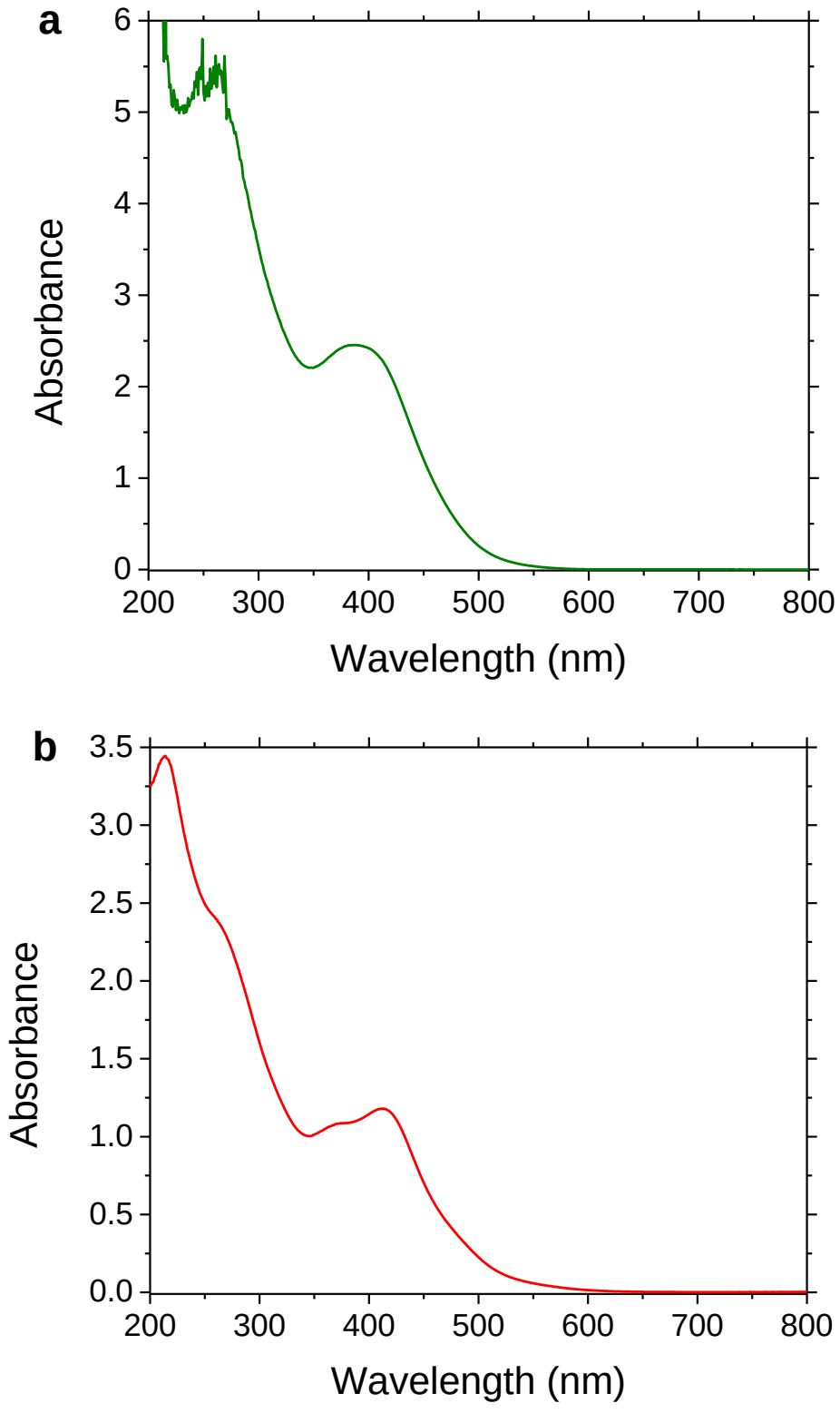

Figure 4.1: Optical Absorbance spectra of $V_3O_7 \cdot H_2O$ nanowires (a) and vanadia/Au nanoconjugates (b).

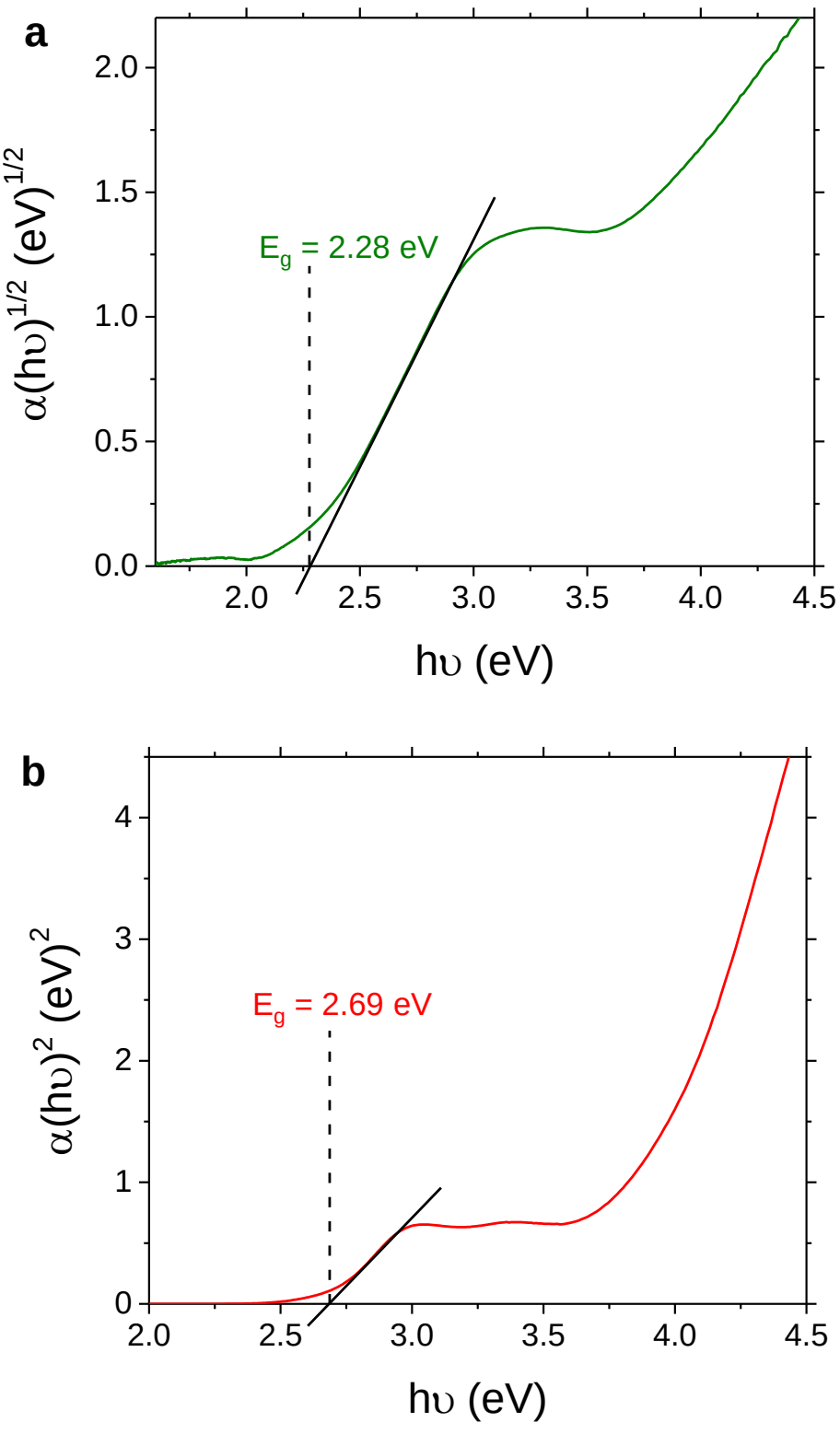

Figure 4.2: Appropriate Tauc plots for $V_3O_7 \cdot H_2O$ nanowires (a) and Au-decorated $V_2O_5 \cdot H_2O$ nanowires (b).

The modification in band gap energy and corresponding transition from an indirect band gap to direct band gap upon Au reduction represents a transformation of $V_3O_7 \cdot H_2O$ to $V_2O_5 \cdot H_2O$. The optical band gap of $V_2O_5 \cdot H_2O$ subsequent to Au reduction is determined to be higher than the minimum energy of 1.5 eV required for photocatalytic splitting of water. Additionally, the derived band gap is well below 3.17 eV, the approximate upper limit of visible light energy. Hence, the photocatalyst employed in the current work possesses a band gap sufficient to absorb visible light energies efficiently and accomplish the redox half-cell reactions for hydrogen generation via water splitting.

4.2 Ultraviolet Photoelectron Spectroscopy

The nanostructures were characterized by ultraviolet photoelectron spectroscopy (UPS) before and after Au reduction using the method detailed in Section 3.2.3. Measurements were performed with the objective of estimating electronic band structures of vanadia before and after Au decoration by determining ionization energies, which is indicative of valence band edge energies in vacuum. UPS scans of $V_3O_7 \cdot H_2O$ and $V_2O_5 \cdot H_2O$/Au nanoconjugates are given by Figures 4.3a and 4.3b, respectively. The derivations of ionization energies, which correspond to valence band edge energies, are also shown in the figures. The valence band edge energies of $V_3O_7 \cdot H_2O$ and $V_2O_5 \cdot H_2O$ NWs are determined to be –8.1 eV and –7.8 eV from the vacuum level, respectively. In the figures, the onsets at –3.2 eV and –3.3 eV are determined as the BE minimum of $V_3O_7 \cdot H_2O$ and $V_2O_5 \cdot H_2O$ electrons, respectively. Additionally a weak band of higher electron energy emission (lower BE) is observed to precede these valence bands of the vanadia structures. Following the literature, this feature is assigned to vanadium 3d states [38]. Although this band is ideally empty and should not yield electron emission, on account of e^- transfer occurring from removed oxygen atoms the oxidation state of some vanadium atoms change from 5 to 4 and the released electrons fill in the vanadium 3d band, which then acts like a heavily-doped conduction band with high population of electrons at its edge. The broadening in

vanadium 3d e^- emission is hypothesized to be due to variation in boundary distance and geometric bonding of V sites [38].

Electron energy band diagram of $V_2O_5 \cdot H_2O$ constructed from the determined valence band edge and band gap energies in the present thesis is shown in Figure 4.4 [39]. Further, the instrumental electron transitions involved in facilitating the redox reactions for photolysis of water using $V_2O_5 \cdot H_2O$/Au photolytic devices are presented on the same energy diagram. The pH of the $V_2O_5 \cdot H_2O$/Au suspensions are found to be 2.4. Since the valence band energy and band gap of $V_2O_5 \cdot H_2O$ are found to be –7.8 eV and 2.69 eV, respectively, its conduction band energy is calculated as $E_c = -7.8 + 2.69 = -5.11$ eV from the vacuum level.

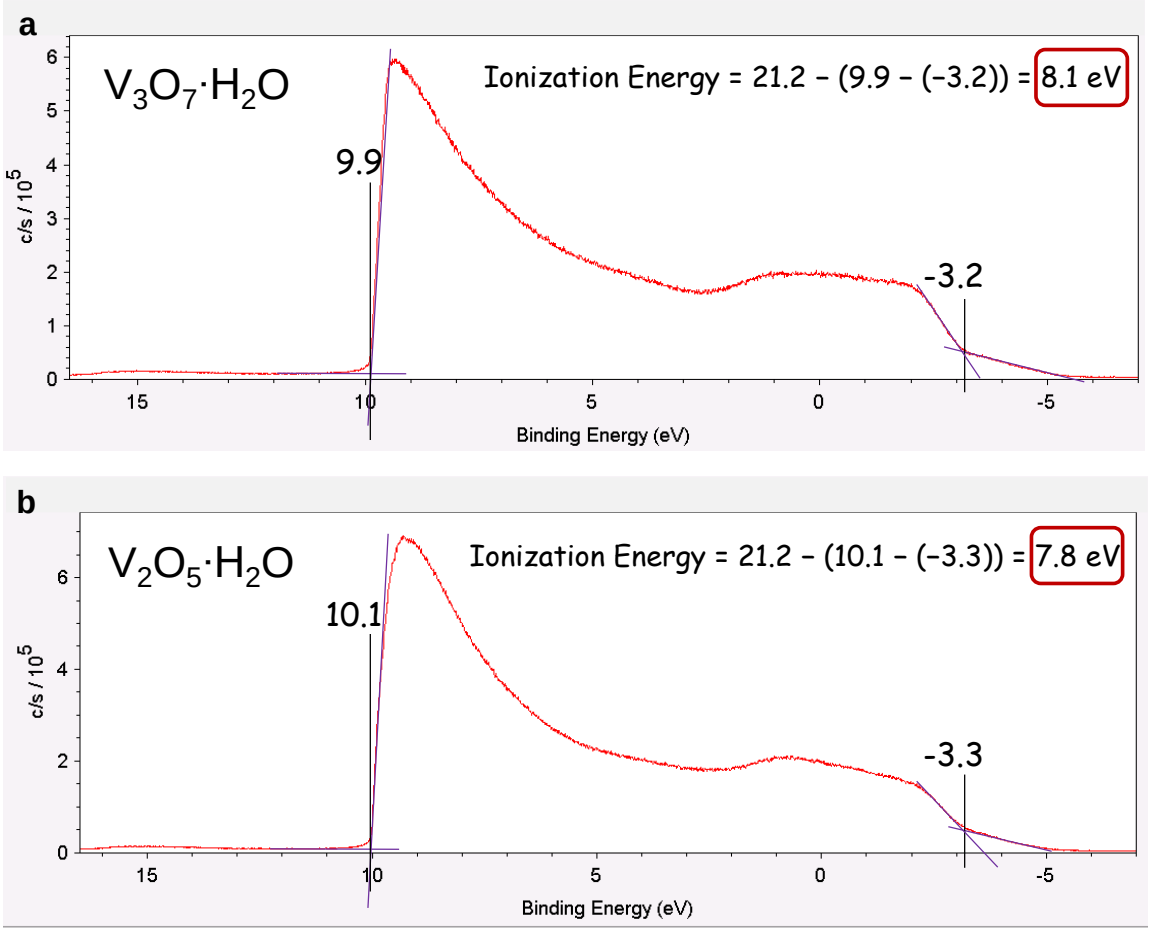

Figure 4.3: Ultraviolet photoelectron spectroscopy scans of $V_3O_7 \cdot H_2O$ nanowires (a) and $V_2O_5 \cdot H_2O$ nanowires decorated with Au nanoparticles (b).

Upon absorption of a photon in vanadia, an e^-/h^+ pair is created. The h^+ diffuses to the interface between vanadia and water for the oxidation of water, which corresponds to an energy of –5.58 eV from vacuum level (at pH = 2.4). Meanwhile, the e^- is transported to Au, which acts as cathode for the photolysis of water and its Fermi level lies at –5.1 eV energy from vacuum level. Au NPs also increase the electro-active surface area for H_2 reduction because of their high surface-to-volume. Accordingly, the overpotential for reduction is expected to be low. On the other hand, overpotential of hydrogen reduction on vanadia is known to be high, thus lowering the photocatalytic efficiency [4].

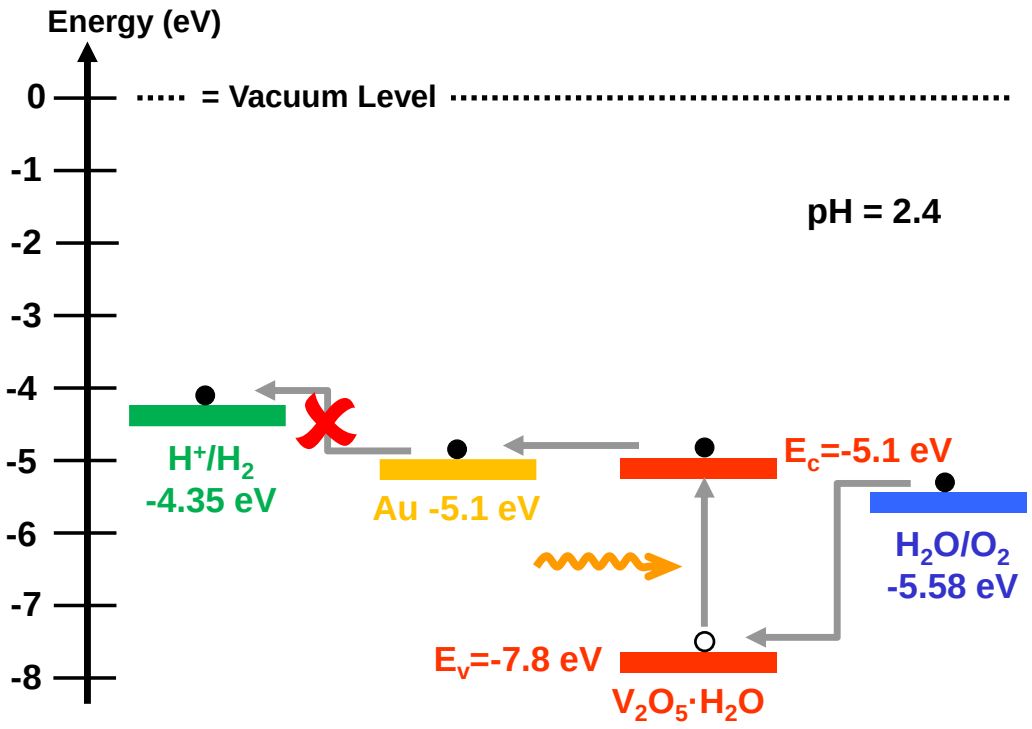

Figure 4.4: Electron energy band diagram of $V_2O_5 \cdot H_2O$ based on UPS findings and electronic transitions required for photocatalytic splitting of water [39, reprinted with permission].

The e^- is then channeled to the H_2 reduction reaction, which requires a minimum potential of –4.35 eV from vacuum level (at pH = 2.4) for the reduction reaction to occur. Evidently, as seen from Fig. 4.4, H_2 generation by H^+ reduction is energetically unfavorable since

H_2 is at a higher reduction potential than Au Fermi level. Hence, one possibility for the observed H_2 evolution may be due to decomposition of the nanostructures. Another possibility can be an organic residue present in water after the synthesis of nanowires. Otherwise the electron energy band structure in Figure 4.4 does not validate water photolysis.

However, there are several factors arguing against the first possibility of decomposition of nanostructures. For instance, the optical band gap of vanadia remains constant during photolysis and H_2:O_2 is produced reproducibly at a stoichiometric ratio of 2.0 ± 0.1 [35]. In addition to these factors, efficient removal of organic residues is accomplished after thorough acetone washing and ambient air drying steps. Morever, supercritical CO_2 drying technique was employed in previous photolysis demonstrations, which is a more efficient approach for the removal of organic residues [35]. Therefore, in order to explain the observed hydrogen generation, lifting up of vanadia and Au NP electron energy levels by a certain negative surface charge is hypothesized. To validate this hypothesis, investigations in the form of cyclic voltammetry was performed for aqueous suspensions of $V_3O_7.H_2O$ nanowires and $V_2O_5{\cdot}H_2O$/Au nanoconjugates.

4.3 Cyclic Voltammetry

In order to verify surface-charge-enabled lifting of electron energy levels in $V_2O_5{\cdot}H_2O$/Au nanoconjugates and explicate the observed hydrogen generation, cyclic voltammetry (CV) measurements were conducted. To validate the reproducibility of the results, 5 cyclic current-voltage measurements each of $V_3O_7{\cdot}H_2O$ and $V_2O_5{\cdot}H_2O$/Au aqueous suspensions were performed. CV has been used extensively as a standard technique in determining HOMO/LUMO levels of organic semiconductors, polymers and other electro-active molecular species for many decades [40, 41, 42, 43]. The method of determining HOMO/LUMO levels is by deriving the onsets of the highest oxidation potential (E_{ox}), which corresponds to HOMO level and highest reduction potential (E_{red}), which corresponds to LUMO level. The difference

between E_{ox} and E_{red} is adopted as the band gap (E_g); i.e., $E_g = E_{ox} – E_{red}$. Similarly, the same technique can be utilized for the determination of conduction bands (E_c), valence bands (E_v) and their corresponding band gaps in inorganic semiconductors [44].

Accordingly, E_c and E_v were estimated by determining the onsets of the highest redox potentials in each measurement. The band gap energy was calculated as the difference between E_v and E_c; i.e., $E_g = E_v – E_c$. Representative CV data for $V_3O_7{\cdot}H_2O$ NWs and $V_2O_5{\cdot}H_2O$ NWs decorated with Au nanoparticles are given by Figures 4.5a and 4.5b, respectively. Additional CV measurements of $V_3O_7{\cdot}H_2O$ and $V_2O_5{\cdot}H_2O$/Au nanostructures are presented in Figures 4.6a, 4.6b, 4.7a, 4.7b, 4.8a, 4.8b, 4.9a and 4.9b. Additionally, the average values of E_c, E_v and E_g with standard deviations from 5 measurements of $V_3O_7{\cdot}H_2O$ NWs and $V_2O_5{\cdot}H_2O$/Au nanoconjugates were calculated in order to evaluate the variance in the results.

In Figure 4.5a, the voltage onsets for reduction and oxidation bands, which are indicative of conduction (E_c) and valance band edge (E_v) energies were determined to be –3.9 and –6.22 eV from vacuum level, respectively. Here, the electron energies were measured against Ag/AgCl reference electrode, but E_v and E_c values were subsequently computed with reference to vacuum level given Ag/AgCl potential is –5.24 eV from the vacuum level. The band gap of $V_3O_7{\cdot}H_2O$ NWs was deduced to be 2.32 eV by calculating the difference between E_v and E_c values; i.e., $E_g = –3.9 – (–6.22) = 2.32$ eV.

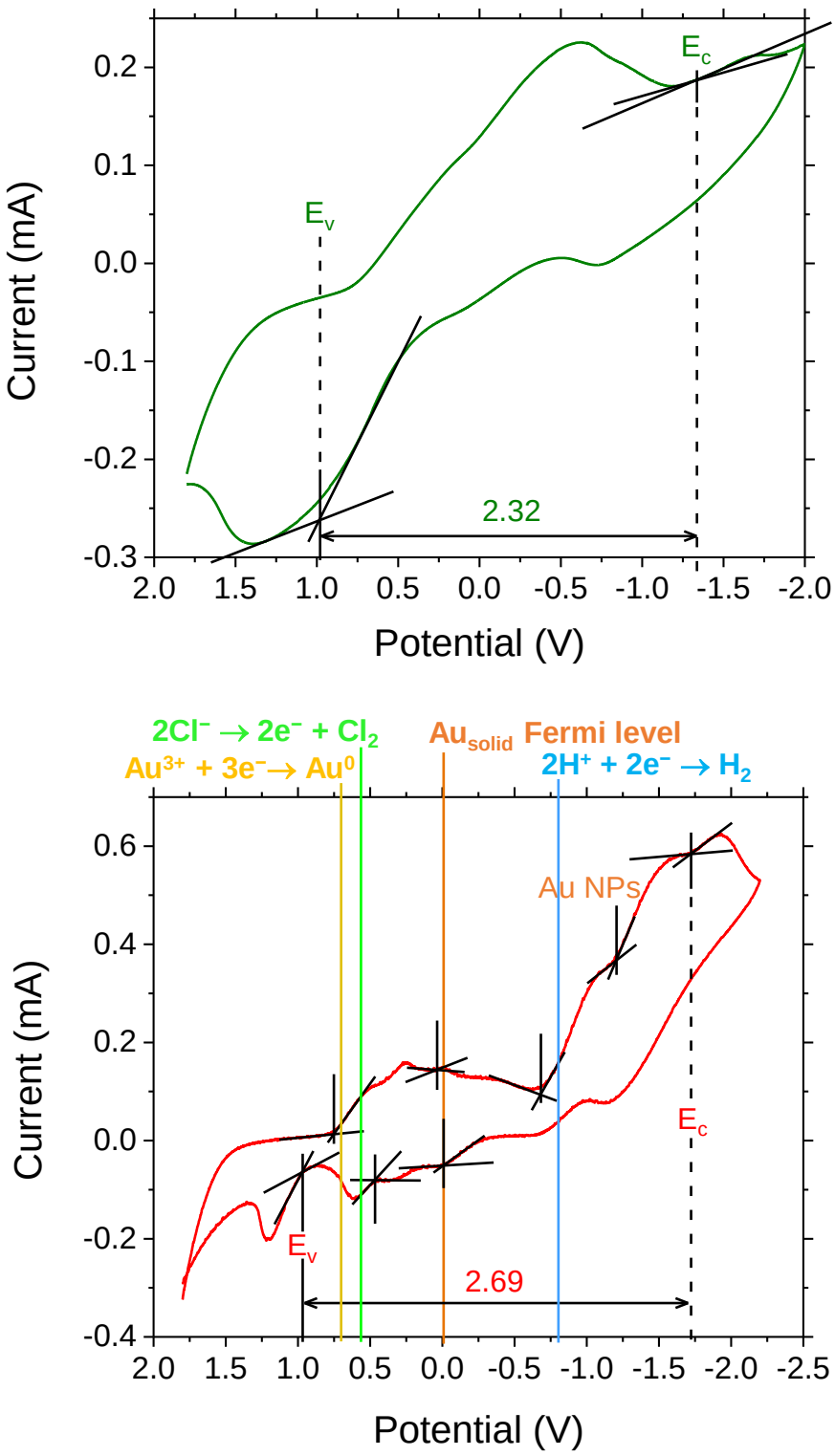

Figure 4.5: CV voltammograms of $V_3O_7 \cdot H_2O$ NWs (a) and Au-decorated $V_2O_5 \cdot H_2O$ NWs (b) (Batch prepared on 10-08-2014 / Measured on 06-03-2015).

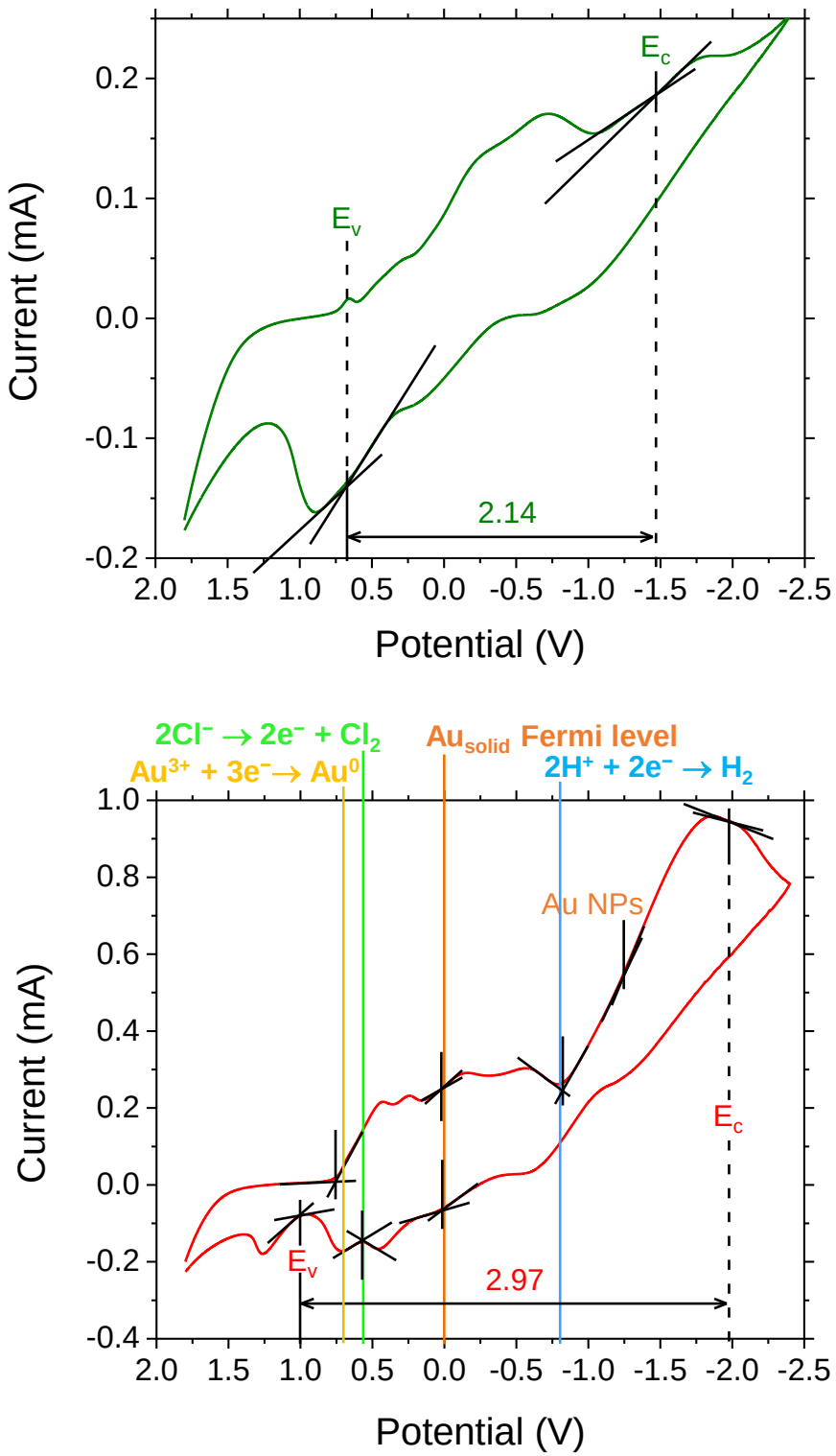

Figure 4.6: Additional measured cyclic voltammograms of $V_3O_7 \cdot H_2O$ NWs (a) and Au-decorated $V_2O_5 \cdot H_2O$ NWs (b) (Batch prepared on 06-23-2014 / Measured on 06-26-2015).

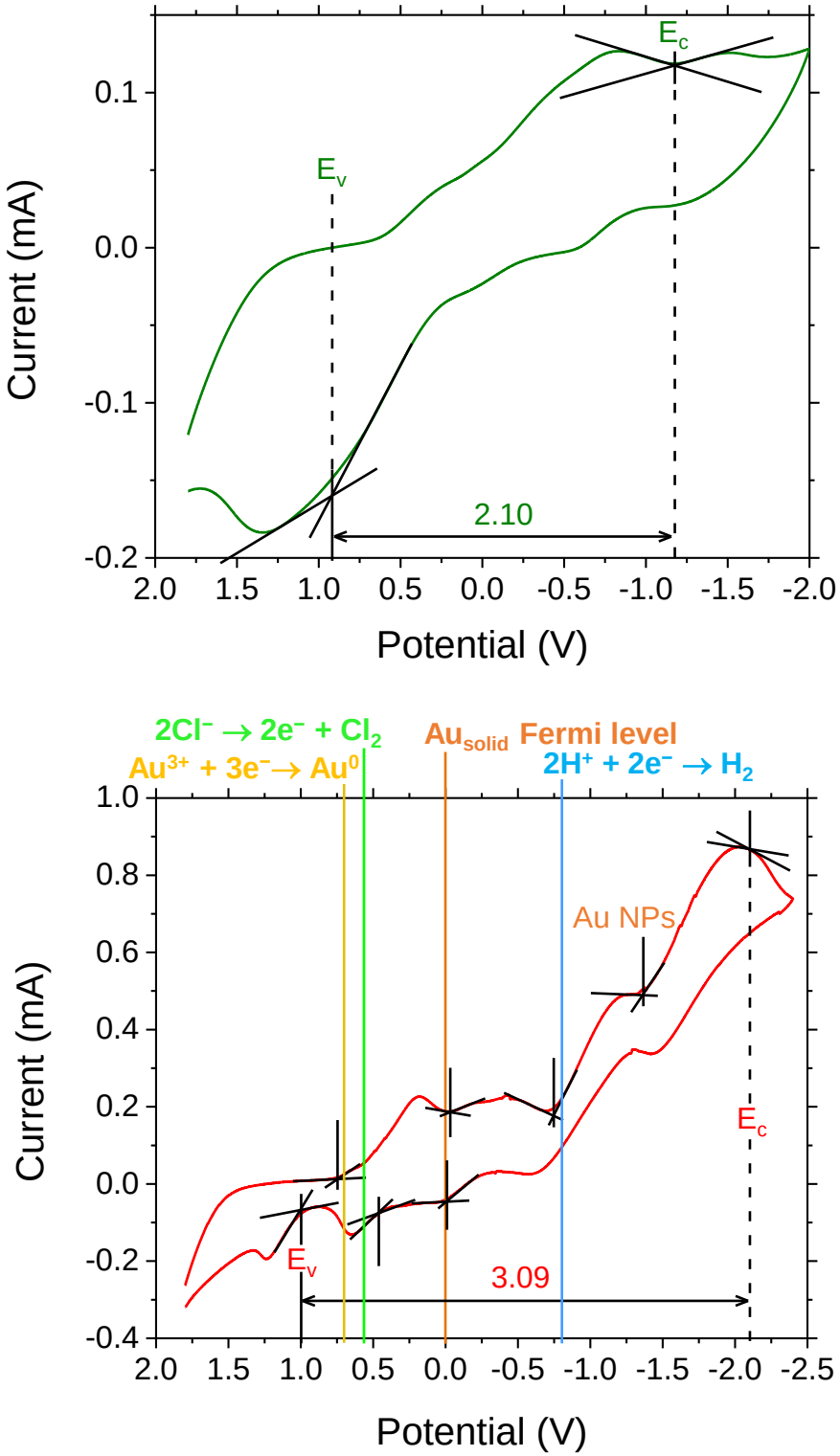

Figure 4.7: Additional measured cyclic voltammograms of $V_3O_7 \cdot H_2O$ NWs (a) and Au-decorated $V_2O_5 \cdot H_2O$ NWs (b) (Batch prepared on 03-09-2015 / Measured on 06-03-2015).

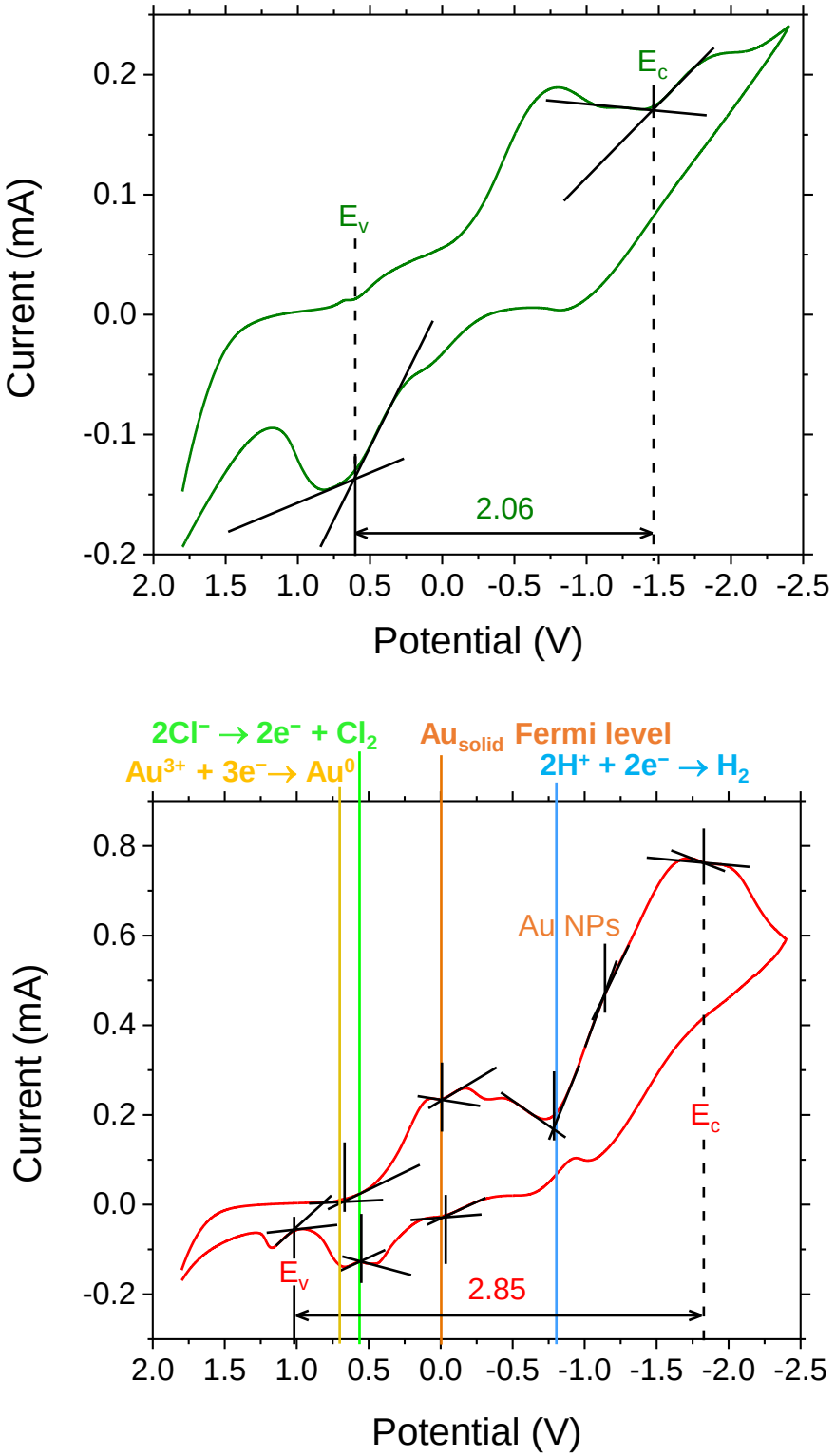

Figure 4.8: Additional measured cyclic voltammograms of $V_3O_7 \cdot H_2O$ NWs (a) and Au-decorated $V_2O_5 \cdot H_2O$ NWs (b) (Batch prepared on 10-08-2014 / Measured on 06-26-2015).

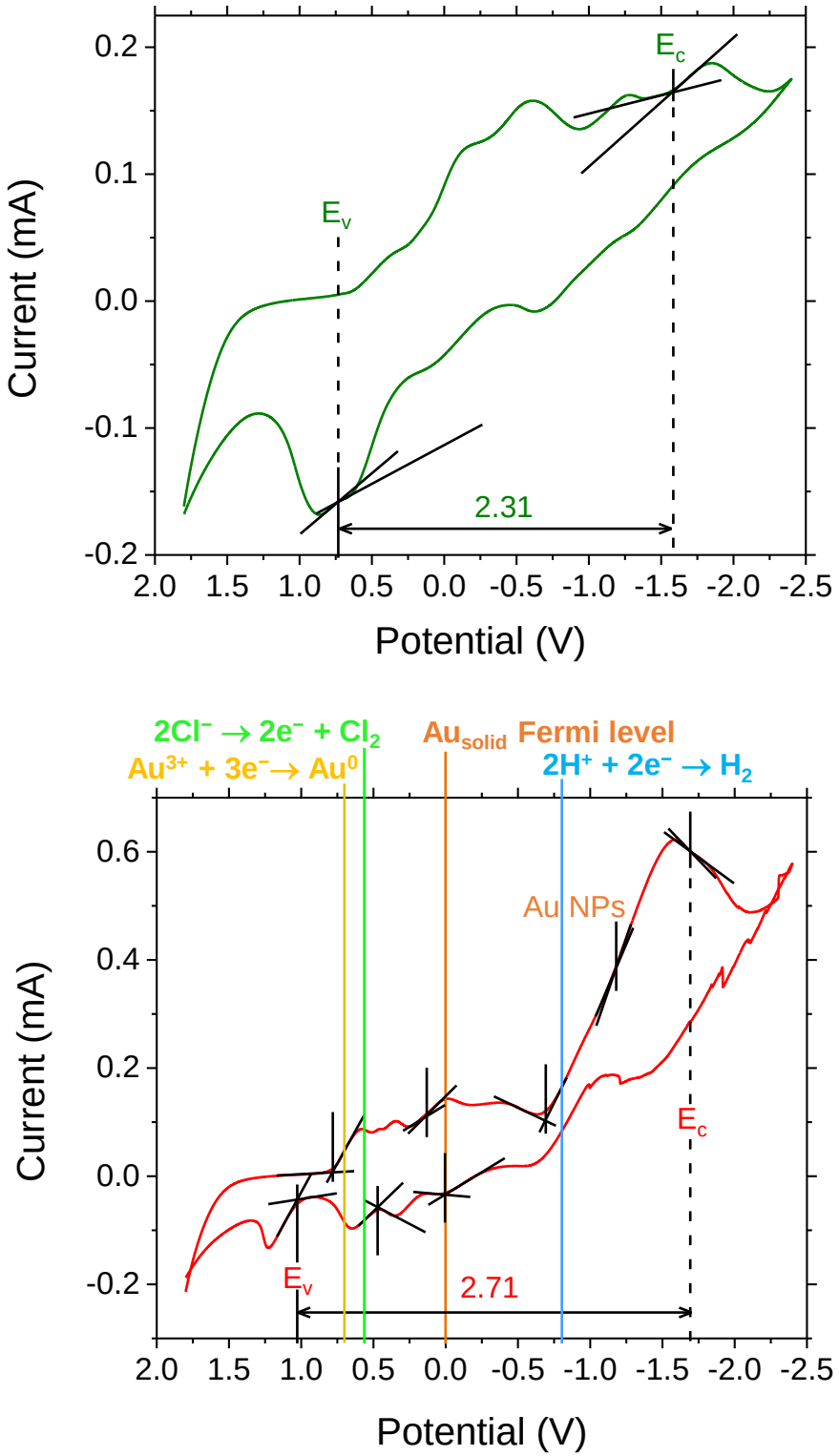

Figure 4.9: Additional measured cyclic voltammograms of $V_3O_7 \cdot H_2O$ NWs (a) and Au-decorated $V_2O_5 \cdot H_2O$ NWs (b) (Batch prepared on 06-23-2014 / Measured on 08-06-2015).

The voltammogram of the conjugates in Figure 4.5b yields conduction band and valence band energy values of –3.52 and –6.21 eV from the vacuum level, respectively. Therefore, the band gap is calculated as the difference between E_v and E_c values; i.e., $E_g = –3.52 – (–6.21) = 2.69$ eV. A good agreement in band gaps measured by CV and optical band gap values measured by Tauc plots is obtained for $V_3O_7{\cdot}H_2O$ NWs as well as $V_2O_5{\cdot}H_2O$/Au nanoconjugates. Further, the voltammogram of the conjugates contains several additional bands, possibly due to the presence of solid Au and residual $HAuCl_4$.

Based on standard electrode potentials, the additional bands are attributed to their corresponding redox reactions as indicated in the figure. Notably, Au reduction on the working electrode is inferred at a potential close to its standard reduction potential of +1.5 eV with respect to SHE or +0.7 eV with respect to the reference electrode (indicated by a yellow vertical line). Au reduction on the working electrode can facilitate subsequent redox reactions. As a matter of fact, one of the reduction bands at approximately +0.8 eV with respect to SHE or 0.0 eV with respect to the reference electrode corresponds to Au Fermi level, possibly due to electron injection into solid Au. Additionally, another band observed at –0.8 eV with respect to Ag/AgCl reference electrode is attributed to H_2 reduction (indicated by a blue vertical line). In the reverse scan, a band observed at +0.56 eV with respect to the reference electrode is attributed to the oxidation of residual $Cl^–$ (indicated by a green vertical line).

Furthermore, another band is observed just below E_c of $V_2O_5{\cdot}H_2O$ at approximately –1.2 eV with respect to the reference electrode, which is attributed to electron injection into the Au NPs conjugated to $V_2O_5{\cdot}H_2O$ NWs. Clearly, the electron energy levels of the nanostructures are observed to be elevated by a certain negative surface charge, when compared to values measured by UPS in vacuum. Hence, the negative surface charge on vanadia also lifts up the energy levels of solid Au in nanoparticles. The negative surface charge facilitates lifting up of the conduction and valence band edge energies in $V_3O_7{\cdot}H_2O$ and Au-decorated $V_2O_5{\cdot}H_2O$ NWs by

approximately 1.9 and 1.6 eV, respectively. The energy shift of 1.2 eV in Au Fermi level in nanoparticles when compared to its neutral Fermi level is also attributed to the negative charge of the NWs. Accordingly, the energy band diagram of Figure 4.4 is revised as in Figure 4.10, in order to explain H_2 generation by H^+ reduction [39]. Based on this revised energy diagram, E_c of $V_2O_5 \cdot H_2O$ and Au Fermi level in nanoparticles are lifted up such that it is at a higher energy level compared to H_2 reduction level. Hence, an electron transferred to Au can be readily channeled to H^+ reduction level for H_2 generation.

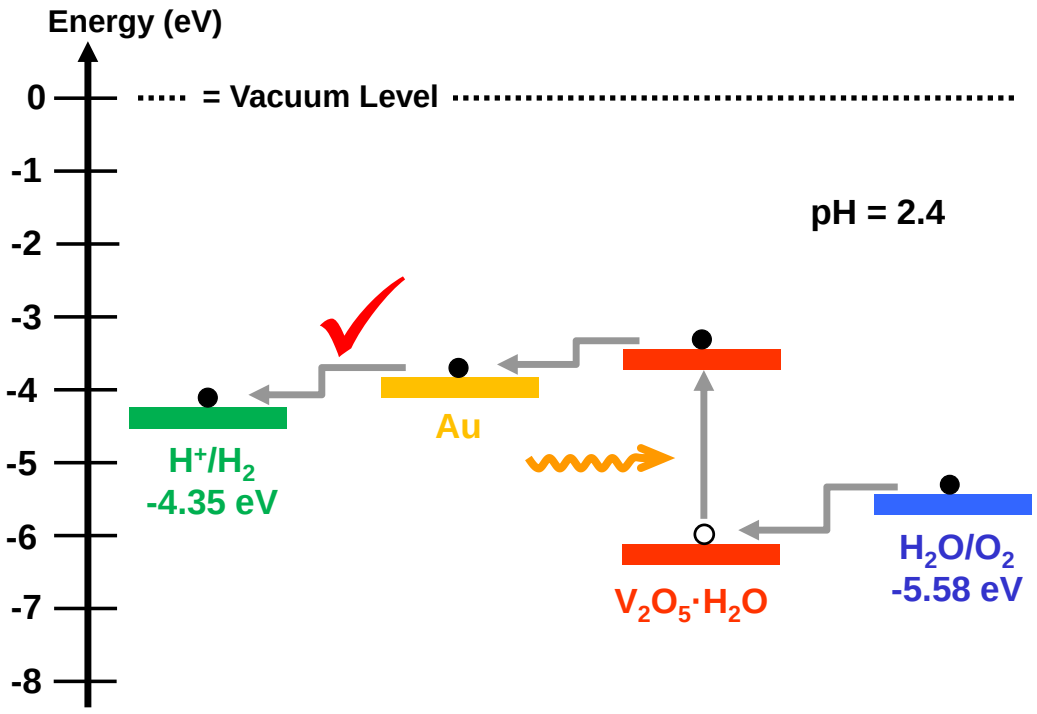

Figure 4.10: Revised electron energy diagram explicating the observed hydrogen generation [39, reprinted with permission].

The average band gaps with standard deviations of $V_3O_7 \cdot H_2O$ NWs and Au-decorated $V_2O_5 \cdot H_2O$ NWs from 5 CV measurements were found to be 2.19±0.122 eV and 2.86±0.171 eV, respectively. The average band gap energy values are in close agreement with optical band gaps measured using Tauc plots.

4.4 Zeta Potential Measurements

A potential reason for alteration of the energy band structure of vanadia in water when compared to that in vacuum is surface charge. To validate this hypothesis, ζ-potentials of vanadia nanowires before and after Au reduction were determined using electrophoresis as detailed in section 3.2.5. ζ-potentials of $V_3O_7{\cdot}H_2O$ NWs and Au-decorated $V_2O_5{\cdot}H_2O$ NWs were determined to be –57.57±1.00 mV and –57.90±2.27 mV, respectively, which are significantly high values. The results are tabulated in Table 4.1 below. High ζ-potential values indicate significant negative surface charge present on the nanostructures and good stability of the aqueous suspensions. The pH values of the aforementioned nanostructures were found to be 2.5 and 2.4, respectively. Hence, the negative surface charge can be attributed to Lewis acid nature of the vanadia NWs, which coordinatively bond with OH^- through sharing the lone e^- pair of oxygen.

Table 4.1: Measured ζ-potentials of the nanostructures.

Nanostructure	ζ-Potential (mV)
$V_3O_7{\cdot}H_2O$ NWs	–57.57±1.00
$V_2O_5{\cdot}H_2O$ NWs + Au NPs	–57.90±2.27

The ζ-potentials and determined E_g and E_v values from CV measurements are summarized in Table 4.2 and compared with results from optical absorption and ultraviolet photoelectron spectroscopy measurements [39].

Table 4.2: ζ-potentials and electron energy band structure parameters of $V_3O_7{\cdot}H_2O$ NWs and Au-decorated $V_2O_5{\cdot}H_2O$ NWs for comparison [39, reprinted with permission].

	$V_3O_7{\cdot}H_2O$ Nanowires	**$V_2O_5{\cdot}H_2O$/Au Nanoconjugates**
ζ-Potential (mV)	−57.57 ± 1.00	−57.90 ± 2.27
Band Gap, Tauc (eV)	2.28	2.69
Band Gap, CV (eV)	2.19±0.122	2.86±0.171
E_v, UPS (eV)	−8.1	−7.8
E_v, CV (eV)	−6.03 ± 0.16	−6.23 ± 0.01

CHAPTER 5

CONCLUSIONS

The following conclusions are deduced from the results of the present work. Recommendations for future research work are also offered.

1. A highly efficient photolytic device comprising vanadia/Au nanoconjugates for H_2 generation was previously demonstrated in the Kalkan Lab. Reproducible light-to-hydrogen conversion and external quantum efficiencies of 5.3% and 11.3% using gas chromatography, respectively, for the first hour of photolysis under 470 nm visible light excitation was evinced [35]. The present thesis further elucidated the mechanism of H_2 generation via water splitting. To this end, investigations in the form of optical absorption spectroscopy, cyclic voltammetry and ultraviolet photoelectron spectroscopy measurements were performed in order to reveal the electronic band structure of the nanostructures in water as well as vacuum.
2. As previously demonstrated in our lab, $V_3O_7{\cdot}H_2O$ nanowires were synthesized using the sol-gel technique and decorated with Au NPs by chemical reduction in the previous thesis work. The band gap of $V_3O_7{\cdot}H_2O$ nanowires was found to be 2.28 eV, which modified to 2.69 eV upon conjugation with Au NPs, as measured using Tauc plots. This change in band gap of vanadia provides a proof of concept for the transformation of $V_3O_7{\cdot}H_2O$ to $V_2O_5{\cdot}H_2O$ after Au decoration in its entire composition. The derived optical band gap

meets the minimum energy requirement of 1.5 eV for photocatalytic splitting of water. Since the determined band gap is less than 3.17 eV, the photocatalyst is also suitable for visible light absorption.

3. The increase of bandgap is because of oxidation of $V_3O_7{\cdot}H_2O$, being the reducing agent for Au reduction, to $V_2O_5{\cdot}H_2O$.
4. The Tauc plots also indicate $V_3O_7{\cdot}H_2O$ is an indirect while $V_2O_5{\cdot}H_2O$ is a direct gap semiconductor.
5. The ionization energies of $V_3O_7{\cdot}H_2O$ and $V_2O_5{\cdot}H_2O$ nanowires were determined to be 8.1 and 7.8 eV using UPS. The conduction band edge of $V_2O_5{\cdot}H_2O$ was estimated to be –5.11 eV from the vacuum level based on the measured valence band edge from UPS and band gap from optical spectroscopy measurements. Accordingly, a discrepancy was observed, that the conduction band edge of $V_2O_5{\cdot}H_2O$ appears to be significantly deeper than the H^+ reduction level of –4.35 eV. Thus, to explain the observed H_2 generation by the nanoconjugates, lifting up of electron energy levels by a certain negative surface charge was hypothesized.
6. To prove the hypothesis of shifting of vanadia electron energy levels in $V_2O_5{\cdot}H_2O$/Au nanoconjugates and further elucidate the mechanism of observed photolytic H_2 generation, cyclic voltammetry (CV) measurements were performed on aqueous suspensions of the nanostructures. The conduction (E_c) and valance band edge (E_v) energies of $V_3O_7{\cdot}H_2O$ nanowires were determined to be –3.9 and –6.22 eV (from vacuum level), respectively. The band gap (E_g) of $V_3O_7{\cdot}H_2O$ was estimated to be 2.32 eV. The E_c and E_v of $V_2O_5{\cdot}H_2O$ nanowires decorated with Au NPs were derived to be –3.52 and –6.21 eV, respectively. The E_g of the nanoconjugates was estimated at 2.69 eV. A remarkable agreement in band gap values measured using CV and optical absorption spectroscopy is obtained. Further, the valence band edges of $V_3O_7{\cdot}H_2O$ nanowires and $V_2O_5{\cdot}H_2O$/Au nanoconjugates were found to be raised by 1.9 and 1.6 eV, respectively,

when compared with values obtained from UPS measurements. Thus, the hypothesis of electron energy levels shifting in order to facilitate the redox reactions for photolytic H_2 generation is validated.

7. To validate the presence of a negative charge responsible for lifting up of electron energy levels in the nanostructures, ζ-potential measurements were conducted using electrophoresis. ζ-potential values of $V_3O_7{\cdot}H_2O$ nanowires and $V_2O_5{\cdot}H_2O$/Au nanoconjugates were determined to be –57.57±1.00 mV and –57.90±2.27 mV, respectively. The significant ζ-potential values indicate the presence of high negative surface charge on the nanostructures, elevating the electron energy levels to facilitate the hydrogen evolution reaction by H^+ reduction. The high ζ-potential values also confirm Lewis acid nature of the NWs, forming coordinative bonds with OH^- adsorbates.
8. The present thesis distinctly elucidates the mechanism of H_2 generation in $V_2O_5{\cdot}H_2O$/Au nanoconjugates. However, in previous photolysis demonstrations in our lab, a degradation in photolysis was observed after 2 hours of operation [8]. Future work must investigate the causes for this degradation. Future work can explore the conjugation of vanadia nanowires with other metals such as Co or Ni in order to improve stability. Au is observed to serve as a suitable co-catalyst and photocathode on account of its suitable Fermi level when compared to H^+ reduction level as well as strong adhesion to vanadia nanowire surfaces. However, residual Cl^- could possibly reduce stability in the conjugates and degrade photolysis. Hence, alternative Au salts like $Au(NO_3)_3$ or $Au(OH)_3$ can be investigated for Au reduction.
9. The present thesis work establishes the importance of surface charge in a photocatalyst. Negative charge is inferred to be instrumental in aligning vanadia electron energy levels with that of redox reactions for photolytic H_2 production. This gained understanding of the photolysis mechanism in $V_2O_5{\cdot}H_2O$/Au nanoconjugates can prove useful in the search for alternative photocatalyst materials as well. Alternate stable photocatalyst materials

with electron energy levels too deep for H_2 generation like WO_3 or Fe_2O_3 can be investigated in an acidic medium to study the effects of surface charge in possibly facilitating H_2 reduction reaction.

REFERENCES

[1] Population Reference Bureau (2015). "2015 World population factsheet." Retrieved December 5, 2014, from http://www.prb.org/pdf15/2015-world-population-data-sheet_eng.pdf.

[2] L. Schlapbach, "Technology: Hydrogen-fuelled vehicles," *Nature,* vol. 460, pp. 809-811, 08/13/print 2009.

[3] "World Energy Resources (WER): 2013 Survey," 23rd edition for the Survey of Energy Resources (SER). Retrieved October, 2013.

[4] M. G. Walter, E. L. Warren, J. R. McKone, S. W. Boettcher, Q. Mi, E. A. Santori, *et al.*, "Solar Water Splitting Cells," *Chemical Reviews,* vol. 110, pp. 6446-6473, 2010/11/10 2010.

[5] A. Fujishima and K. Honda, "Electrochemical Photolysis of Water at a Semiconductor Electrode," *Nature,* vol. 238, pp. 37-38, 07/07/print 1972.

[6] H. Kato, K. Asakura, and A. Kudo, "Highly Efficient Water Splitting into H_2 and O_2 over Lanthanum-Doped $NaTaO_3$ Photocatalysts with High Crystallinity and Surface Nanostructure," *Journal of the American Chemical Society,* vol. 125, pp. 3082-3089, 2003/03/01 2003.

[7] K. Maeda, K. Teramura, D. Lu, T. Takata, N. Saito, Y. Inoue, *et al.*, "Photocatalyst releasing hydrogen from water," *Nature,* vol. 440, pp. 295-295, 03/16/print 2006.

[8] Sean K. Maclaskey, "Nanowire-nanoparticle conjugate photolytic devices for renewable hydrogen production," Master's Thesis, Oklahoma State University 2011.

[9] Z. Zou and H. Arakawa, "Direct water splitting into H_2 and O_2 under visible light irradiation with a new series of mixed oxide semiconductor photocatalysts," *Journal of Photochemistry and Photobiology A: Chemistry,* vol. 158, pp. 145-162, 6/2/ 2003.

[10] Z. Zou, J. Ye, K. Sayama, and H. Arakawa, "Direct splitting of water under visible light irradiation with an oxide semiconductor photocatalyst," *Nature,* vol. 414, pp. 625-627, 12/06/print 2001.

[11] A. Grimes, S. Ranjan, and O. K. Varghese, “Light, Water, Hydrogen,” Springer Science+Business Media, LLC, New York, NY 10013, USA 2008

[12] F. E. Osterloh, "Inorganic Materials as Catalysts for Photochemical Splitting of Water," *Chemistry of Materials,* vol. 20, pp. 35-54, 2008/01/01 2008.

[13] H. Park, Y. Park, W. Kim, and W. Choi, "Surface modification of TiO_2 photocatalyst for environmental applications," *Journal of Photochemistry and Photobiology C: Photochemistry Reviews,* vol. 15, pp. 1-20, 6// 2013.

[14] J. Georgieva, E. Valova, S. Armyanov, N. Philippidis, I. Poulios, and S. Sotiropoulos, "Bi-component semiconductor oxide photoanodes for the photoelectrocatalytic oxidation of organic solutes and vapours: A short review with emphasis to TiO_2–WO_3 photoanodes," *Journal of Hazardous Materials,* vol. 211–212, pp. 30-46, 4/15/ 2012.

[15] M. Zhang, Z. Cui, X. Yang, Q. Wei, and S. Zhu, "CdS sensitized nanoporous TiO_2/CuO layer prepared by dealloying of Ti–Cu amorphous alloy," *Materials Letters,* vol. 80, pp. 131-134, 8/1/ 2012.

[16] J. Kim, D. W. Hwang, H. G. Kim, S. W. Bae, J. S. Lee, W. Li, *et al.*, "Highly Efficient Overall Water Splitting Through Optimization of Preparation and Operation Conditions of Layered Perovskite Photocatalysts," *Topics in Catalysis,* vol. 35, pp. 295-303.

[17] T. T. Le, M. S. Akhtar, D. M. Park, J. C. Lee, and O. B. Yang, "Water splitting on Rhodamine-B dye sensitized Co-doped TiO_2 catalyst under visible light," *Applied Catalysis B: Environmental,* vol. 111–112, pp. 397-401, 1/12/ 2012.

[18] J. Zhu and M. Zäch, "Nanostructured materials for photocatalytic hydrogen production," *Current Opinion in Colloid & Interface Science,* vol. 14, pp. 260-269, 8// 2009.

[19] J. Jitputti, Y. Suzuki, and S. Yoshikawa, "Synthesis of TiO_2 nanowires and their photocatalytic activity for hydrogen evolution," *Catalysis Communications,* vol. 9, pp. 1265-1271, 3/31/ 2008.

[20] E. Pulido Melián, O. González Díaz, A. Ortega Méndez, C. R. López, M. Nereida Suárez, J. M. Doña Rodríguez, *et al.*, "Efficient and affordable hydrogen production by water photo-splitting using TiO_2-based photocatalysts," *International Journal of Hydrogen Energy,* vol. 38, pp. 2144-2155, 2/19/ 2013.

[21] H. Kadowaki, N. Saito, H. Nishiyama, H. Kobayashi, Y. Shimodaira, and Y. Inoue, "Overall Splitting of Water by RuO_2-Loaded $PbWO_4$ Photocatalyst with $d^{10}s^2$-d^0 Configuration," *The Journal of Physical Chemistry C,* vol. 111, pp. 439-444, 2007/01/01 2007.

[22] Y. Wang, Z. Zhang, Y. Zhu, Z. Li, R. Vajtai, L. Ci, *et al.*, "Nanostructured VO_2 Photocatalysts for Hydrogen Production," *ACS Nano,* vol. 2, pp. 1492-1496, 2008/07/01 2008.

[23] A. Kudo and I. Mikami, "Photocatalytic activities and photophysical properties of $Ga_{2-x}In_xO_3$ solid solution," *Journal of the Chemical Society, Faraday Transactions,* vol. 94, pp. 2929-2932, 1998.

[24] K. Maeda, K. Teramura, D. Lu, T. Takata, N. Saito, Y. Inoue, *et al.*, "Photocatalyst releasing hydrogen from water," *Nature,* vol. 440, pp. 295-295, 03/16/print 2006.

[25] A. Kudo and M. Sekizawa, "Photocatalytic H_2 evolution under visible light irradiation on $Zn_{1-x}Cu_xS$ solid solution," *Catalysis Letters,* vol. 58, pp. 241-243.

[26] C.-C. Wu, H.-F. Cho, W.-S. Chang, and T.-C. Lee, "A simple and environmentally friendly method of preparing sulfide photocatalyst," *Chemical Engineering Science,* vol. 65, pp. 141-147, 1/1/ 2010.

[27] Z. Liu, W. Hou, P. Pavaskar, M. Aykol, and S. B. Cronin, "Plasmon Resonant Enhancement of Photocatalytic Water Splitting Under Visible Illumination," *Nano Letters,* vol. 11, pp. 1111-1116, 2011/03/09 2011.

[28] T. Hisatomi, K. Maeda, K. Takanabe, J. Kubota, and K. Domen, "Aspects of the Water Splitting Mechanism on $(Ga_{1-x}Zn_x)(N_{1-x}O_x)$ Photocatalyst Modified with $Rh_{2-y}Cr_yO_3$ Cocatalyst," *The Journal of Physical Chemistry C,* vol. 113, pp. 21458-21466, 2009/12/24 2009.

[29] N. Bao, L. Shen, T. Takata, and K. Domen, "Self-Templated Synthesis of Nanoporous CdS Nanostructures for Highly Efficient Photocatalytic Hydrogen Production under Visible Light," *Chemistry of Materials,* vol. 20, pp. 110-117, 2008/01/01 2008.

[30] P. Wu, J. Shi, Z. Zhou, W. Tang, and L. Guo, "$CaTaO_2N$–$CaZrO_3$ solid solution: Band-structure engineering and visible-light-driven photocatalytic hydrogen production," *International Journal of Hydrogen Energy,* vol. 37, pp. 13704-13710, 9// 2012.

[31] S. P. Meshram, P. V. Adhyapak, U. P. Mulik, and D. P. Amalnerkar, "Facile synthesis of CuO nanomorphs and their morphology dependent sunlight driven photocatalytic properties," *Chemical Engineering Journal,* vol. 204–206, pp. 158-168, 9/15/ 2012.

[32] D. Jiang, H. Zhao, Z. Jia, J. Cao, and R. John, "Photoelectrochemical behaviour of methanol oxidation at nanoporous TiO_2 film electrodes," *Journal of Photochemistry and Photobiology A: Chemistry,* vol. 144, pp. 197-204, 11/7/ 2001.

[33] M. R. Hoffmann, S. T. Martin, W. Choi, and D. W. Bahnemann, "Environmental Applications of Semiconductor Photocatalysis," *Chemical Reviews,* vol. 95, pp. 69-96, 1995/01/01 1995.

[34] A. A. Nada, H. A. Hamed, M. H. Barakat, N. R. Mohamed, and T. N. Veziroglu, "Enhancement of photocatalytic hydrogen production rate using photosensitized TiO_2/RuO_2-MV^{2+}," *International Journal of Hydrogen Energy,* vol. 33, pp. 3264-3269, 7// 2008.

[35] A. K. Kalkan, "Nanowire–nanoparticle conjugate photolytic device," *Nanomaterials and Energy,* vol. 1, pp. 159-167, 2012.

[36] Ç. Ö. Topal, S. Tan, H. Lu, N. Leventis, and A. K. Kalkan, "Resonant Two-Photon Oxidation in Vanadium Oxyhydrate Nanowires above a Threshold Laser Intensity," *The Journal of Physical Chemistry C,* vol. 116, pp. 10186-10192, 2012/05/10 2012.

[37] G. Teran-Escobar, J. Pampel, J. M. Caicedo, and M. Lira-Cantu, "Low-temperature, solution-processed, layered V_2O_5 hydrate as the hole-transport layer for stable organic solar cells," *Energy & Environmental Science,* vol. 6, pp. 3088-3098, 2013.

[38] Q.-H. Wu, A. Thissen, W. Jaegermann, and M. Liu, "Photoelectron spectroscopy study of oxygen vacancy on vanadium oxides surface," *Applied Surface Science,* vol. 236, pp. 473-478, 9/15/ 2004.

[39] S. Varghese, C. Walgama, M. Wilkins, S. Krishnan, and K. Kalkan, "Surface-Charge-Enabled Photolytic Hydrogen Generation in $V_2O_5{\cdot}H_2O$/Au Nanoconjugates," *MRS Advances,* vol. FirstView, pp. 1-6, 2016.

[40] L. Leonat, G. Sbarcea, and I. V. Branzoi, "Cyclic voltammetry for energy levels estimation of organic materials," *UPB Sci Bull Ser B,* vol. 75, pp. 111-118, 2013.

[41] A. Shafiee, M. M. Salleh, and M. Yahaya, "Determination of HOMO and LUMO of [6, 6]-phenyl C61-butyric acid 3-ethylthiophene ester and poly (3-octyl-thiophene-2, 5-diyl) through voltametry characterization," *Sains Malaysiana,* vol. 40, pp. 173-176, 2011.

[42] S. Admassie, O. Inganäs, W. Mammo, E. Perzon, and M. R. Andersson, "Electrochemical and optical studies of the band gaps of alternating polyfluorene copolymers," *Synthetic metals,* vol. 156, pp. 614-623, 2006.

[43] S. Janietz, D. Bradley, M. Grell, C. Giebeler, M. Inbasekaran, and E. Woo, "Electrochemical determination of the ionization potential and electron affinity of poly (9, 9-dioctylfluorene)," *Applied physics letters,* vol. 73, pp. 2453-2455, 1998.

[44] S. N. Inamdar, P. P. Ingole, and S. K. Haram, "Determination of Band Structure Parameters and the Quasi-Particle Gap of CdSe Quantum Dots by Cyclic Voltammetry," *ChemPhysChem,* vol. 9, pp. 2574-2579, 2008.

VITA

Sunith Varghese

Candidate for the Degree of

Master of Science

Thesis: SURFACE-CHARGE-TUNED VANADIA NANOWIRE PHOTOLYTIC HYDROGEN GENERATORS

Major Field: Mechanical and Aerospace Engineering

Biographical:

Personal Data:

Born on November 20, 1991, in Pathanamthitta, Kerala, India.

Education:

Completed the requirements for the Master of Science in Mechanical & Aerospace Engineering at Oklahoma State University, Stillwater, Oklahoma in July, 2016.

Completed Bachelor of Technology in Mechanical Engineering at Jawaharlal Nehru Technological University, Hyderabad, India in May, 2013.

Experience:

Worked as a Research Assistant under Dr. A. Kaan Kalkan in the Functional Nanomaterials Laboratory at Oklahoma State University, Stillwater, OK.

Worked as a Teaching Assistant for Materials Science course from Aug., 2015–May, 2016 under Dr. A. Kaan Kalkan & Dr. James E. Smay in the Mechanical & Aerospace Engineering department at Oklahoma State University, Stillwater, OK.

Worked as a Teaching Assistant for Basic Instrumentation, Applied Fluid Mechanics and Statics courses from Aug., 2014–May, 2015 under Prof. Ken Belanus & Prof. Aaron Alexander in the Mechanical Engineering Technology department at Oklahoma State University, Stillwater, OK.